The Pennsylvania State University
The Graduate School
College of Engineering

MODELING, DESIGN AND TESTING OF A MULTI-CELL PERIODIC FLUIDIC FLEXIBLE MATRIX COMPOSITE DEVICE

A Thesis in
Aerospace Engineering
by
Bondoux Alexandre

Submitted in Partial Fulfillment
of the Requirements
for the Degree of

Master of Science

December 2015

The thesis of Bondoux Alexandre was reviewed and approved* by the following:

Edward C. Smith
Professor of Aerospace Engineering
Thesis Advisor, Chair of Committee

Christopher D. Rahn
Professor of Mechanical Engineering
Thesis Advisor

Michael M. Micci
Director of Graduate Studies
Professor of Aerospace Engineering

*Signatures are on file in the Graduate School.

Abstract

Vibrations have been a growing concern in recent years. Previously considered as a by-product of performance, they are now seen as an important topic to satisfy customer requests for comfort. Therefore, substantial efforts have been put into the reduction of such incommodities.

Vibrations are mechanical waves that are produced by many different physical phenomena. They usually transport a low amount of energy, but the human body perceives them extremely well up to a few thousand Hertz. Over time, they can also provoke fatigue phenomena in material, that can lead to failure. Making the vibrations completely disappear is usually impossible. Instead we try to reduce their intensity to such a level that their impact becomes negligible.
Mitigating vibration can be easy if you do not have too many constraints on the final product. However, our case will emphasize helicopter applications, especially noise in the cabin.

One could think that shielding the cabin with layers and layers of elastomeric materials are well suited, but helicopters have a very sensitive weight budget. These machines usually have a very limited payload in comparison to other transportation systems. Therefore, we need to concentrate on devices that would reduce

the vibrations with a minimal weight penalty. However, studies have proven that most of the intensity of vibrations in helicopter is produced by a discrete set of physical phenomena, generating a reduced set of frequencies. Typically, around a dozen of sharp peaks are seen on frequency spectra. Consequently, our interest has been focused on anisotropic vibration reduction systems that could satisfy the above requirements.

The present work is extending our knowledge of some fluidic devices called F^2MC tubes, standing for Fluidic Flexible Matrix Composite tubes. They consist of a highly anisotropic Flexible Matrix Composite (FMC) laminate that surrounds a working fluid. The FMC is a composite shell having reinforcement oriented with a specific angle with respect to the longitudinal axis. These tubes have proven to be efficient at reducing vibrations in some specific configurations, being able to be tuned to target a given frequency quite accurately. As a consequence, the next move has been to try to miniaturize these tubes, providing interesting structural stiffness and vibration damping abilities. The idea would be to connect back to back a given number of small sized F^2MC tubes, called "cells", in a periodic structure. The damping effect would them sum up and produce a band gap centred on a frequency of choice, determined by the properties of cell.

First, we explore how F^2MC tubes work. The basic principles are outlined with some performance results. We show the challenges that come with such small scale, high aspect ratio device.

Secondly, we present the work that was done on a previous model of the tubes developed at Penn State to give the users abilities to speed up computations and increase the overall accuracy. Finely tuning its physical parameters leads to per-

formance improvements.

Thirdly, with that tool in hand we move on to the concept of multi cells F^2MC tubes, comparing it to the single cell tube. This is aimed at paving the way for a future meta material that would contain dozens or maybe hundreds of F^2MC cells embed in a material, yielding a stop band that could target multiple toxic frequencies at a time. At the same time, the high static stiffness necessary in helicopters would be conserved.

Multiple F^2MC tubes were built at Penn State Mechatronic Research Laboratory (MRL). They were experimentally tested and their performance were compared to previous F^2MC versions and theoretical predictions. While the results match for a low amount of cells, results start diverging between the model and the experiment results as soon as the number of periodic cells increase in the system.

Table of Contents

List of Figures

List of Tables

Acknowledgments

This project could never have happened without the help of many people.
First I would like to thank my advisers Dr. Edward Smith and Dr. Christopher Rahn for their guidance during these two years at Penn State. They hosted me in their laboratories and provided me with all the advice and materials I could need to pursue my Master of Science. I cannot keep going either without mentioning the support of LORD Corporation, who funded me the whole time and provided me with high performance fluid to run my experiments. They gave me an amazing professional experience and insight of the company during my summer 2014 internship, and I thank them for that too. I would like to address a special thank to Dr. Jose Palacios whose expertise in LabView helped me learn a lot about this critical software in data acquisition.

In the MRL, I met a lot of smart and really helpful people. Kentaro Miura, Shawn Treacy and Matt Krott, thanks for your continuous help with all the laboratory equipments. You helped me more than once getting started with how things worked in the MRL. Thanks to all my labmates and colleagues Jun Ma, Mayank Garg, Tahzib Safwat, Tanvir Tanim, Xiaokun Ma.
I would like to thank my mother for her unconditional help and support through all these years, making my dream to go study in the United States a reality.

Chapter 1
Introduction

1.1 Background in helicopter interior noise

1.1.1 Source of the noise

The main source of discomfort for passengers in a helicopter is the high level of noise in the cabin. Helicopter pilots and passengers see their abilities to communicate with each other reduced, fatigue increases and alertness is reduced, potentially endangering the whole crew in a demanding situation, as described by Pollard [2].

Most of the noise come from the gearbox of the aircraft, localized right above the head of the passengers. This is a key element in comparison to other transport systems: in a plane, the gearbox would be close to the engine, far away from the cabin; in a car it is enclosed in the front part of the car. If the system is not too much dependent on the weight, the gearbox would usually be shielded from the outside world by layers of cheap insulator.

In our case, let's have a look at the life cycle of the noise. Many different parts create them, but for humans the most annoying one originate from the gears. Even with the best lubrication systems, the friction between them creates noises that

are transmitted two ways to the cabin:

- through the struts that hold the gearbox and connect it to the cabin. They are usually made out of stiff materials given that they need to be able to hold the whole helicopter during any flight manoeuvre,

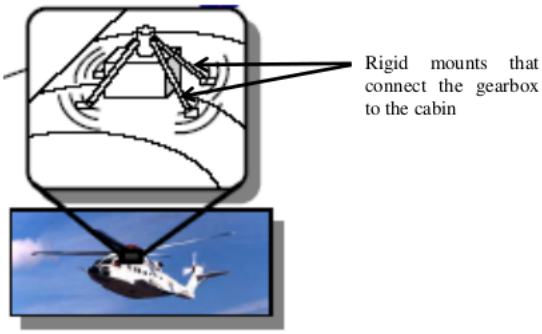

Figure 1.1. Rigid mounts transmit noise through the struts(Szefi, [1])

- airborne, via the gearbox resonating like a bell. The noise is transmitted through the air and make the cabin ceiling resonate.

A deeper look at the gearbox shows that gear-reducing stages and their bearings generate most of the noises. They are surrounded by a metal casing that amplifies the noise as described above. A description is given in the following picture.

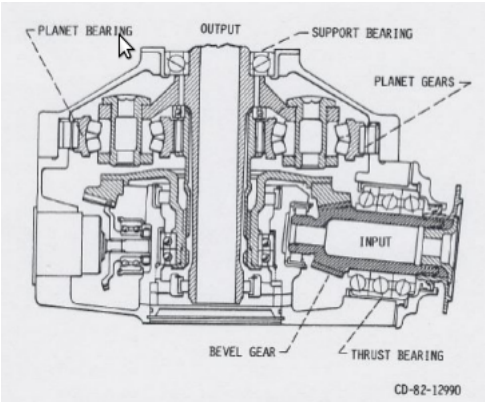

Figure 1.2. Gearbox of an OH 58C, Pollard [2]

The engine powers the shaft which rotates at high speed. Then, gears are needed to reduce that to accommodate for the main rotor, the rear rotor and the alternator that powers the embedded electric systems. But since the the gear alignments are never perfect, forces are generated randomly on the gears that excite their resonance frequencies. Then, the bearings carry these frequencies that are sent to the struts and the housing. Next, the noises are radiated from the gearbox or transmitted via the rigid connections to the cabin. Let's sum up the noise paths with the following picture:

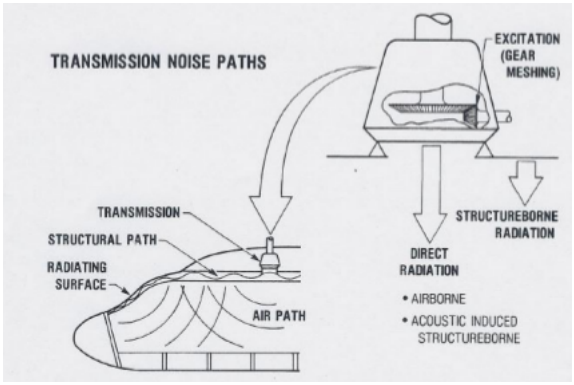

Figure 1.3. Ways for the noises to get into the cabin [2]

The consequences can be significant in terms of noise for the people inside the cabin, depending on the cruise conditions. Generally speaking, the higher the misalignment of the gears the higher the forces generated and the louder the noise. A smaller acoustic volume, meaning a smaller cabin volume, will also increase the noise.

Eventually, a noise level comprised between 85 dB and 115 dB is reached, mainly due to a few selected frequencies. Even if this is physically more annoying that broadband noise, it is completely different in the way that provided an accurate targeting of a few tones, huge reductions in the overall noise can be achieved. Let's have a look at two example spectra, one from Sikorsky and another one from

Augusta Westland:

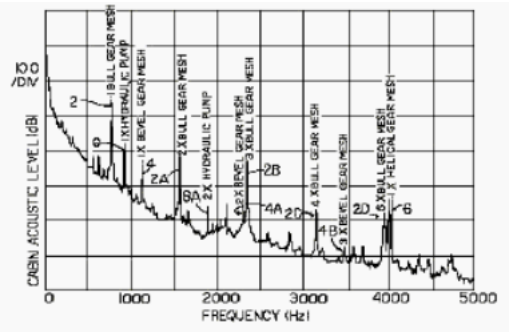

Figure 1.4. Spectrum of a Sikorsky S-76 helicopter

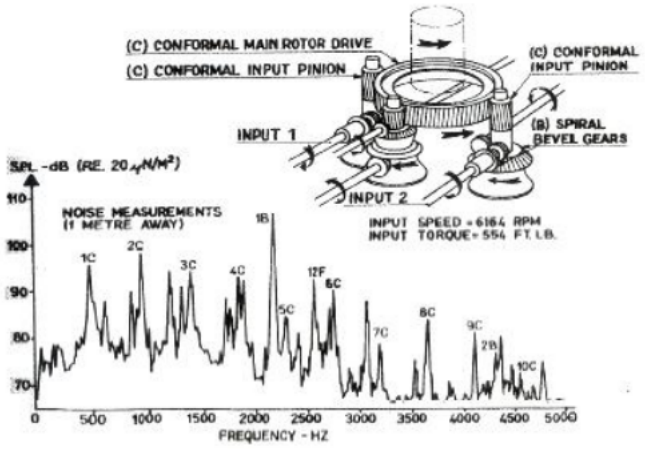

Figure 1.5. Spectrum of an Agusta Westland Lynx helicopter

Clearly, a selected number of frequencies is at the origin of most of the noise.

1.1.2 Reducing the noises

There are many ways to reduce the overall noise level. It can be reduced at the source, the gears, or apply sound treatments on the cabin and/or the mounting struts. Let's have a brief overview of the different possible solutions.

1.1.2.1 Improving the gear geometry

Here the target is the source of the noise. Some of the work has been done on optimizing the gear geometry to have minimal source strengths [2]. However, this has a limit and at some point researchers shifted their attention toward alternative strategies that would aim at taking into account the fact that the system will not be perfect. For instance, maximization of gear contact ratio, reduction in transmission errors and minimization of tooth deflection were investigated by Coy et al. [6], Rosen and Frint [7]. High Contact Gearing (HCGRG) is mentioned as a technique allowing two full gear teeth to be in contact at any time, with reduced deflections and higher contact area. However, whatever the design used, manufacturing tolerances are usually an important parameter in the overall noise level radiated.

1.1.2.2 Shielding the inside of the cabin

Additionally to reduce the noise at the source, the cabin can be shielded. Marze et al [8] describe the procedure in three steps:
- diagnosis of the situation,
- design of a soundproofing system,
- validation of the design.

Even if this sounds easier than carefully designing the gears, it is most of the time a solution that translates into an elevated weight penalty. Traditionally, foams, blankets, acoustic barriers are used to attain a 15-20 dB reduction in military aircraft and a 25-30 dB reduction in civil aircraft according to Pollard [2]. It can be pushed to up to 25-35 dB according to Hartman [9] or Levin [10] but extremely careful seals are needed and the weight of these treatments soars up to 3% of the gross weight, a really high figure when compared to the actual maximum payload weight.

1.1.2.3 Gearbox struts

Last, the struts can be isolated from the cabin. The usual target is the connection between the struts and their attachment point where elastomeric isolators can be mounted. But there is here a narrow design margin given that a high stiffness must be ensured at all time, enough to support the whole weight of the aircraft multiplied by the maximum acceleration factor allowed in flight.

Some products try to answer this issue by stacking up layers of rubber with metal plates: called High Capacity Laminate, they manage to provide a good balance between high load abilities and noise damping capacities.

Ideally, the frequency response of the struts would look like:

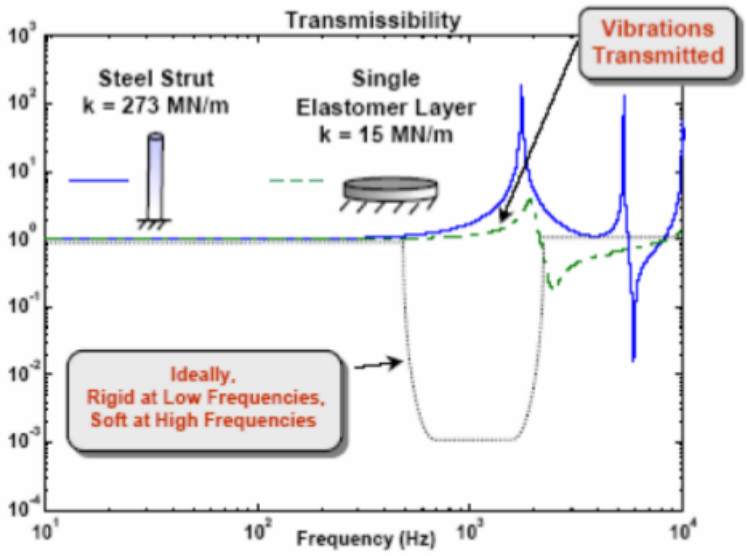

Figure 1.6. Ideal struts response [1]

In grey is the ideal behaviour of the struts: after a given cut off frequency,

there is a huge bandgap that prevents noises from propagating. Then, at really high frequencies the struts start transmitting again but this is of less a concern given that the human ear cannot hear anything there and the energy carried by the noise waves is pretty low. In blue is the transmissibility of an usual steel strut. In green is the result achieved with a single layer elastomer. Some additional work is indeed needed to reduce the transmissibility to a minimal range.
Szefi [1] worked on an efficient multi-layered isolator that could target high frequency noises in helicopter cabin by embedding a solution in the mounting struts.

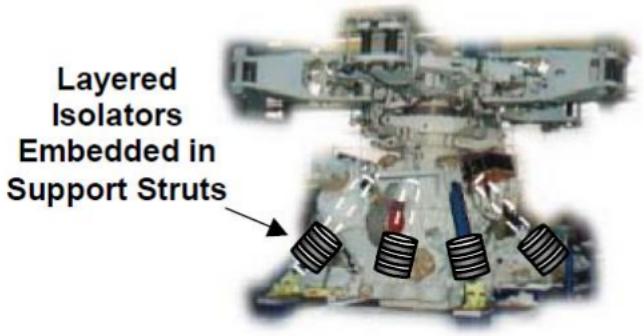

Figure 1.7. Ideal struts response [1]

The cylindrical isolator provided the following drop in transmissibility:

A fair decrease in transmissibility for frequencies around 800 Hz to 3000 Hz can be seen. The fluidic isolators seemed to be a good approach to explore further.

1.1.2.4 Active damping treatments

The last category of solutions consists of the active dampers. Passive solutions are most of the time designed to target a specific flight environment and can lack flexibility. This is definitely an area of improvement that could be the purpose of an active system. Therefore researchers have tried to reduce the noise in the cabin thanks to the combined use of microphones and loudspeakers [11]. The principle

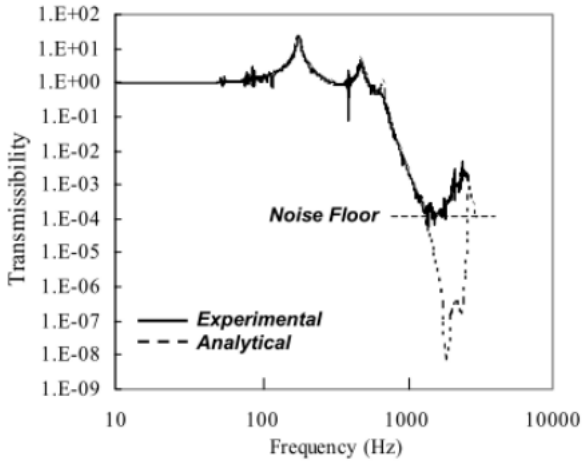

Figure 1.8. Transmissibility of a three cells system, by Szefi [1]

is pretty simple: microphones detect incoming waves and loudspeakers radiate the same wave, out of phase with the first one to cancel it. However, this is a really sensitive solution that quickly needs a lot of microphones and speakers. Global control starts to be tricky at really high frequencies due to the large amount of modes to cope with. Engineers at Sikorsky [12], EADS [13] and Westland [14] have tried this with some degree of success.

To conclude, many different solutions have been used to reduce the overall noise level in a helicopter so far. However, there is still room for improvements, leading to the need for a low power, light weight and cost effective device. A system that combines the previous good points was then choosen: the F^2MC tubes.

1.2 Background in F^2MC tubes

There are two categories of actuators of interest in noise science for us: these which are electrically driven and the fluid driven ones. When electrically driven, such as piezoelectric ceramic based, magnetostrictive alloy based or shape memory

polymer based, they provide good actuation performance. Fluid powered actuators have a much higher power density and energy density(Zupan, [15]) and have consequently recently received serious interest. However they have a few non negligible drawbacks, like need for pressurization, plumbing, pistons, valves and precise seals. The Fluidic Flexible Matric Composite tries to get the best out of these by removing the need for a pumping piston, therefore getting rid of any wear, leakage of frictions that is usually involved. Moreover, the emphasize is on working on reduced scale to be pave the way for a future hydraulic smart structure.

When not filled, the tube consists of a fibre mesh embedded in an elastomeric matrix. Depending on the angle of the fibres regarding the axial direction, the tube will either contract or expand when an axial force is applied. As a general rule, Philen et al. showed that a winding angle of less than 55° leads to contraction of the tube when stretched and an angle of more than 55° leads to expansion of the tube [3].

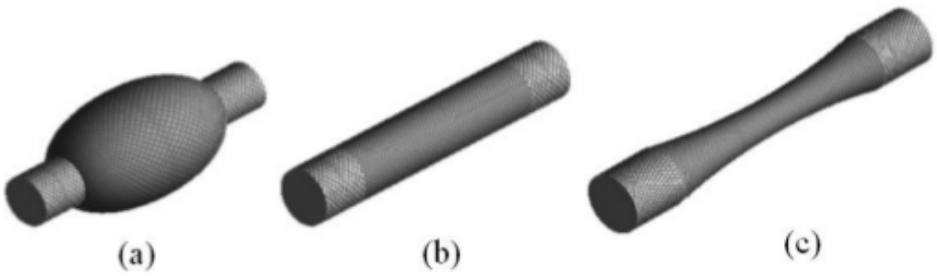

Figure 1.9. (a) Pressurized tube with an angle of less than 55°, (b) Tube at rest, (c) Pressurized tube with an angle of more than 55° [3]

A nonlinear elastic model was developed by Liu and Rahn [16] which predicts the contraction and elongation of such a tube under pressurization. For a small applied pressure, large displacements can be observed.

F^2MC tubes share some properties with McKibben actuators, including the

high power-to-weight ratio and low cost. But their geometric properties can be more accurately controlled than the usual braided sleeve/rubber design of a McKibben actuator. Furthermore, multi-layered F^{2}MC tubes with different winding angle for each layer and/or extremely small angles could be envisionned. They are difficult to achieve with a McKibben actuator. The F^{2}MC tube therefore adds a layer of tunability to fluidic systems.

1.3 Custom properties

Two extreme configurations bind the F^{2}MC tube range of performances: when the tube is sealed and when it's completely open.

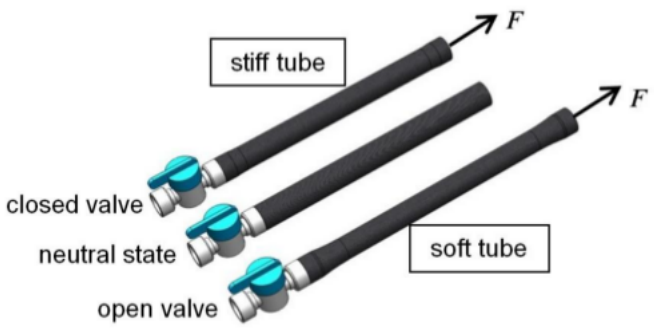

Figure 1.10. Extreme configurations of a tube [4]

When stretched, the tube will contract. If the tube is in an "open" configuration, meaning that one end is fully open, then the stiffness is moderate and the fluid is pumped out of the tube. If the tube is in a "sealed" configuration, meaning that both ends are completely sealed, then the stiffness is much higher. Between these two, a wide range of performances can be achieved. Shan et al. discussed the nonlinear axisymetric deformation of an F^{2}MC tube using large deformation theory [17]. Philen et al. used shell theory to get the effective stiffness of such a tube for open and closed valve configuration [3]. Shan et al. then added compliances

from the different parts of the system [18]. Controlling the fluid flow is here the main target, and they demonstrated that one could modify the angle of the fibres and/or the properties of the matrix to obtain the best performances in a given configuration. Eventually, Zhang et al. managed to design and build an artificial fish driven by F^2MC actuators [19], showing how promising this technology could be for future applications.

1.4 Application of the F^2MC tube to noise reduction

Multiple studies have been performed on the abilities of the F^2MC tube to reduce noises. Zhu et al. worked on a rigid matrix made of polyurethane filled with different fluids, achieving a pumping ability over 100 times higher than what could have been done with a piston of the same diameter [4] for a given axial force. Then, more work was done by Wimmer et al. to take into account shear lag and effect in tubes of finite length [16]. This allowed us to build a more accurate model of the frequency response of the F^2MC tubes.

When noises stretch the tube, the inner fluid is pumped in and out. There is a transfer of mechanical energy from the noises to the fluid. Then, the energy of the fluid is dissipated by viscosity on the inner walls of the tube. Consequently, the high pumping abilities of the tubes is a tremendous asset to efficiently dissipate the energy. Lotfi-Gaskarimahalle et al. showed that adding an external extension to the pumping element that is the F^2MC tube can reduce the noise at a selected frequency. This additional tube is called an "inertia track" given that it adds inertance (fluid inertia) to the hydraulic circuit. Then, Scarborough et al. demonstrated that F^2MC tubes have interesting capacities as noise isolators on load carrying structures [20]. Philen tuned the resonant frequency and damping performance through the use of an end valve [3]. Last, Zhu developed had an

analytical and experimental approach to structure integrated F^{2}MC tubes [4].

1.5 Working with frequency responses

Most of the analytical and the experimental work was done using modal analysis of a system. This is aimed at getting the dynamic characteristics of a system like natural frequencies, damping, mode shapes...etc [21]. A shaker provokes an excitation by applying a sinusoidal force with a shifting frequency and an impedance head combining acceleration and force transducers measures the output. Given that they are most of the time piezoelectric sensors, the static variables cannot be accessed with this method. A static load cell was then used with a laser to get the response to static loads.

The shaker is controlled by the main computer and a DAC (Digital to Analog Converter). Then, a ADC (Analog to Digital Converter) is used to sample the data from the sensors and send them back to the main computer where they can be interpreted([22], [23]).

1.6 Present work

The purpose of this work is to develop a large stopband F^{2}MC tube. According to what has been seen, F^{2}MC tubes usually have the ability to target a specific frequency but have troubles having a wider damping area. Previous models are then refined and lead to the frequency response prediction of multi-cells F^{2}MC tubes. Various number of cells of different geometric properties are designed, built and tested on a longitudinal set up. Our goal is to validate the new model between the range of 100 Hz to 1000 Hz, where most of the noise is carried.

Regarding the inner fluid, multiple of them will be tested and compared to see what can get the best performance out of the device. This also includes considerations about long term storage, re-usability and low toxicity.

In Chapter 2 is discussed the correction brought to the initial model. In Chapter 3 is detailed the experiments done for multi-cells F^2MC tubes. Lastly, Chapter 4 concludes the work.

Chapter 2
Additional corrections to the initial model

2.1 Expanding the initial model to a multi-tube configuration

Zhu [4] derived a model for a pack[1] of F^{2}MC tubes working in a specific configuration [4]. It mainly involved modelizing the tube as a pressurized, homogeneous orthotropic cylinder undergoing an axial force. The axissymetric stress and strain distribution was found using Lekhnitskii's solution [24]. Additionally, the lamina is assumed transversely isotropic, leading us to deal with five independent elastic constants: the longitudinal Young's modulus E_1, the transverse Young's modulus E_2, two Poisson's ratio ν_1 and ν_2 and one shear modulus G_{12}.

The model accounted for tubes that would be clamped on a cantilever beam. A shaker would then apply a sweep in frequency to the tip of the beam in order to get the frequency response.

[1] A pack of tubes consists of n tubes in parallel, having the same fixation positions

However, the model was only used to predict the performance of one pack of tubes on the cantilever beam. This was efficient at targeting one specific frequency but would not yield the best results if two or multiple frequencies had to be targeted.

Therefore,the model is extended to N-packs of tubes on a cantilever beam. This system would then target N frequencies.
Every time the model is run, the equations are solved the following way:
The cantilever beam is split in 2N+1 1-D areas on the beam, N being the number of packs of tubes.

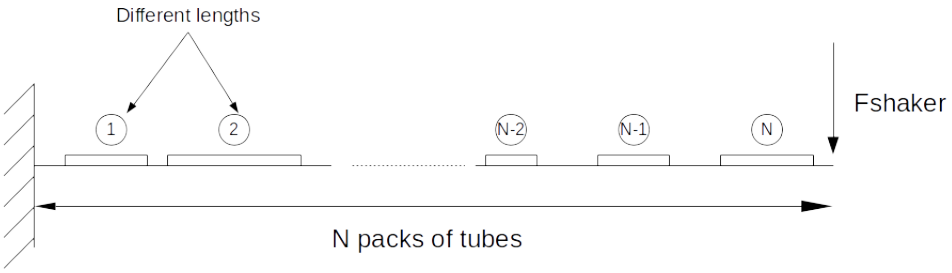

Figure 2.1. A cantilever beam with N packs of tubes on it

These tubes share the same physical properties but the length. Besides the root and the tip in $x = 0$ and $x = L$ (L being the length of the cantilever beam), each boundary corresponds to a point where a tube is applying a moment on the beam. The following conditions are applied at the tip and the root :

$$w(0) = 0 \tag{2.1}$$

$$w'(0) = 0 \tag{2.2}$$

$$w''(L) = 0 \tag{2.3}$$

$$w'''(L) = 0 \tag{2.4}$$

with w being the vertical displacement with respect to the rest position.

2.1.1 2 pack configuration

The following changes were made to the original code:

i) Another volume is introduced in the system: the one coming from the second tube.

$$V_0 = \pi a_0^2 (y_1 - x_1) \tag{2.5}$$

becomes:

$$V_1 = \pi a_0^2 (y_1 - x_1)$$
$$V_2 = \pi a_0^2 (y_2 - x_2)$$

With V the volume of the tube, a_0 the inner diameter, x_1 and y_1 the position of the beginning and the end of the first tube ($0 \leq x_1 \leq y_1 \leq$ L), x_2 and y_2 the position of the beginning and the end of the second tube ($0 \leq x_2 \leq y_2 \leq$ L).

ii) The fluid flow is found by:

$$Q = -\mathring{\Delta}_f = \left(\frac{\Delta V}{V_0} + \frac{P_1}{B_w} \right) N V_0 \tag{2.6}$$

Zhu [4] showed that the changed in volume can be linked to the axial strain ϵ_z and

the azimuthal strain ϵ_θ:

$$\frac{\Delta V}{V_0} = \epsilon_z + 2\epsilon_{\theta|_{r=a_1}} \tag{2.7}$$

Higher order strains are neglected. These two strains can be expressed in terms of force applied and pressure in the tube:

$$\epsilon_z = \varphi_1 F_s + \varphi_2 P_1 \tag{2.8}$$

$$\epsilon_{\theta|_{r=a_1}} = \varphi_3 F_s + \varphi_4 P_1 \tag{2.9}$$

The φ_k terms depend of the geometry of the tube. The different terms can now be grouped to obtain the expression of the fluid flow:

$$Q = -N\left(\varphi_1 + 2\varphi_3\right) V_0 \mathring{F}_s - N\left(\varphi_2 + 2\varphi_4 + \frac{1}{B_w}\right) V_0 \mathring{P}_1 \tag{2.10}$$

Two parameters that will be present in the following developments are identified:

$$Sq = -V_0(\varphi_1 + 2\varphi_4) \tag{2.11}$$

$$Tq = -V_0\left(\frac{1}{B_w} + \varphi_2 + 2\varphi_5\right) \tag{2.12}$$

In the 2 tubes model these two equations become:

$$Sq_1 = -V_1(\varphi_1 + 2\varphi_4)$$

$$Tq_1 = -V_1\left(\frac{1}{B_w} + \varphi_2 + 2\varphi_5\right)$$

$$Sq_2 = -V_2(\varphi_1 + 2\varphi_4)$$
$$Tq_2 = -V_2\left(\frac{1}{B_w} + \varphi_2 + 2\varphi_5\right)$$

where B_w is the bulk modulus of water[2] and $(\varphi_i)_i$ coefficients depending on the geometry of the tubes computed by the code.

iii) Two equations are added to close the system. First, the pressure of the accumulator P_a can be related to the flow rate Q.

$$P_1 - P_a = \frac{1}{C_d}Q \tag{2.13}$$

where C_d is the flow coefficient. Secondly the variation of pressure in the accumulator can be expressed as a function of the fluid flow:

$$\frac{dP_a}{dt} = \frac{1}{C_a}Q \tag{2.14}$$

iv) The transfer function is the ratio of the complex strain ϵ_z to the longitudinal force F_t. It leads to:

$$TS = \frac{(Ca\ s + Cd)(\varphi_1 - \varphi_2 Sq) - \varphi_1 CaCd/n}{n(Ca\ s + Cd)(Tq + Sq\pi a_0^2) - CaCd} \tag{2.15}$$

Two other parameters based on the transfer function can also be defined for simplification:

[2]Other liquids will be considered later

$$G_{x_1} = \frac{TS(x_1 - y_1)}{d^2} \tag{2.16}$$

$$G_{s_1} = G_{x_1} EIl \tag{2.17}$$

where d is the distance between the centerline of the tube and the neutral axis of the beam. With the two tube configuration:

$$\begin{cases} TS_1 = \dfrac{(Ca\ s + Cd)(C_1 Tq_1 - C_2 Sq_1) - C_1 CaCd/n_1}{n_1(Cas + Cd)(Tq_1 + Sq_1 \pi a_0^2) - CaCd} \\ TS_2 = \dfrac{(Cas + Cd)(C_1 Tq_2 - C_2 Sq_2) - C_1 CaCd/n_2}{n_2(Cas + Cd)(Tq_2 + Sq_2 \pi a_0^2) - CaCd} \\ G_{x_1} = \dfrac{TS_1(x_1 - y_1)}{d^2} \\ G_{x_2} = \dfrac{TS_2(x_2 - y_2)}{d^2} \\ G_{s_1} = G_{x_1} EIl \\ G_{s_2} = G_{s_1} EIl \end{cases}$$

where n_k is the number of tubes in pack k.

The expression of the reaction moment applied by each tube to the cantilever beam has been found. However, three different situations can be encountered (See Figure 2.2):

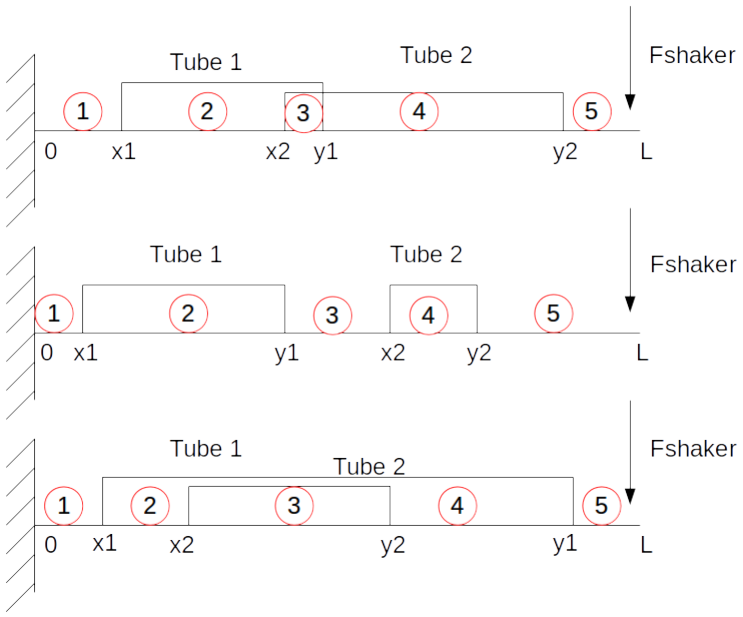

Figure 2.2. Three different configurations in a 2-pack system

The resolution of the different configuration are quite the same. From the first one can be deduced the others. This is the one developed here.

For section $i \in [[1;5]]$, the vertical displacement is of the following form:

$$w_i(x) = A_i sin(\lambda x) + B_i cos(\lambda x) + C_i sinh(\lambda x) + D_i cosh(\lambda x) \tag{2.18}$$

where

$$\lambda^4 = -\frac{s^2 \rho A + sC}{EI} \tag{2.19}$$

with:

$s = j\omega$ in [rad/s],

ρ the density [kg/m^3],

C the dissipation coefficient [kg/s],

E Young's modulus [Pa],

I the area moment of inertia [m^4]

It yields a way bigger matrix that can be found in Annex A.

It features:

- 2 conditions at the root of the cantilever beam,
- 4 continuity equations at the beginning of the first tube,
- 4 continuity equations at the end of the first tube,
- 4 continuity equations at the beginning of the second tube,
- 4 continuity equations at the end of the second tube,
- 2 conditions at the tip of the beam.

Adding only one pack of tube makes the matrix quite consequent. It can then be solved for the coefficients of $w(x)$ in any area. Eventually, the theoretical displacement at the tip of the cantilever beam, $w(L)$, is found.
There are two other possible matrices for the two other tube configurations, depending on the relationships between x_1, x_2, y_1, y_2. Applying the same procedure allows us to come to the same conclusions.

2.1.2 N-pack configuration

Predicting the behaviour of N packs of tubes on the beam is done in the same way. First, the beam is split in 2N+1 areas. The same equation is used to describe the displacement at a given point on the beam. Each section will have 4 coefficients to

be determined. Then, is applied the set of limit conditions: 2 at the root, 4 at each interface with a tube and 2 at the tip. The matrix containing all the equations is solved for the coefficients of the tip area.

2.2 Donovan's correction

2.2.1 Modifications

The model can now fit any number of packs of tubes. Regarding the fluid flow, two parameters are critical. There is the resistance R and the inertance I. Previous estimations of the resistance had used a mix of Poiseuille's flow and a correction based on the Reynold's number. Regarding the inertance, it was completely based on Poiseuille's flow. Results were decent but the Reynold's number had to be tuned to fit the experiment. The best match was obtained around $R_e = 2000$, which sounded acceptable but lacked of physical background to explain the value. Therefore, one tuned parameter was eliminated by applying another theory describing the evolution of these two coefficients with frequency. Here are the previous values for the resistance and the inertance:
Reynold's number:

$$R_e = 2000$$

Custom resistance expression:

$$R_f = \left(1 + 4.56 r_0 \frac{R_e}{64L}\right) \frac{8\mu l}{\pi r_0^4}$$

Compensative term:

$$R_z = 2.5\ 10^{10}$$

Final resistance:

$$R_{circuit} = R_f + R_z$$

Inertance:

$$I = \frac{\rho l}{\pi r_0^2} \tag{2.20}$$

Donovan et al. [5] developed in 1991 a model for an oscillating fluid in small tubes. They showed that the flow can be described through the use of a single non-dimensional parameter α given by:

$$\alpha = r_0 \sqrt{\frac{\omega}{\nu}} \tag{2.21}$$

where:
r_0 is the inner radius of the tube [m],
ω is the damped natural frequency of oscillations [rad/s],
ν is the kinematic viscosity [m^2/s]

However, it's tough to have access to the inertance through α alone. Therefore another parameter, β, was introduced as a parallel of α but for known quantities in the system. The only distinction is that it takes into account the undamped natural frequencies instead of the damped one:

$$\beta = r_0 \sqrt{\frac{\omega_n}{\nu}} \tag{2.22}$$

where:

r_0 is the inner radius of the tube [m],

ω_n is the undamped natural frequency of oscillations [rad/s],

ν is the kinematic viscosity [m^2/s]

Based on these parameters, here is an expression for R:

$$R = \begin{cases} \dfrac{8\mu l}{\pi r_0^4} & \text{for } \alpha < 2 \\ \dfrac{8\mu l}{\pi r_0^4}\ 0.166\ \alpha^{1.49} & \text{for } \alpha > 10 \end{cases} \tag{2.23}$$

To access the value of the inertance, there is a three steps procedure to follow. First, retrieve the of β thanks to the $\frac{\alpha}{\beta}$ vs β curve.

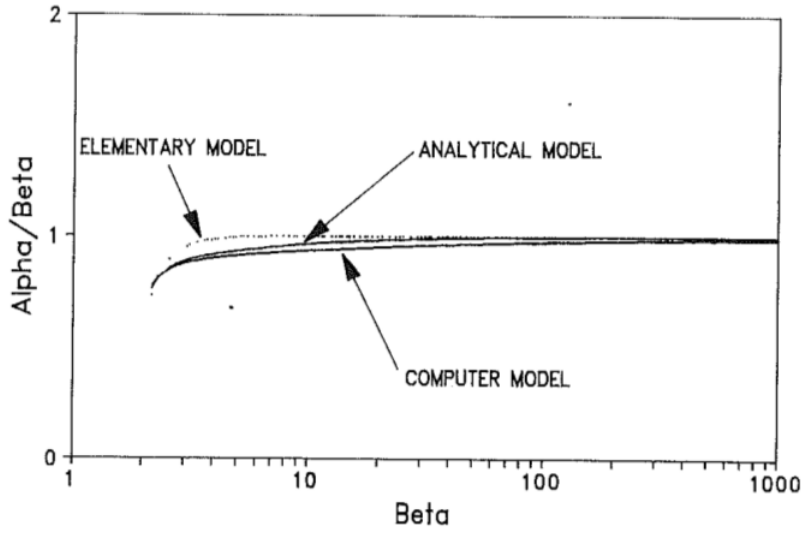

Figure 2.3. Experimental $\frac{\alpha}{\beta}$ vs β [5]

There is a slight difference between Poiseuille's model, referred as elementary model, and the more realistic results of the computer simulation.

Secondly, access to the value of the dimensionless inertance I_0 through the I_0 vs β

curve.

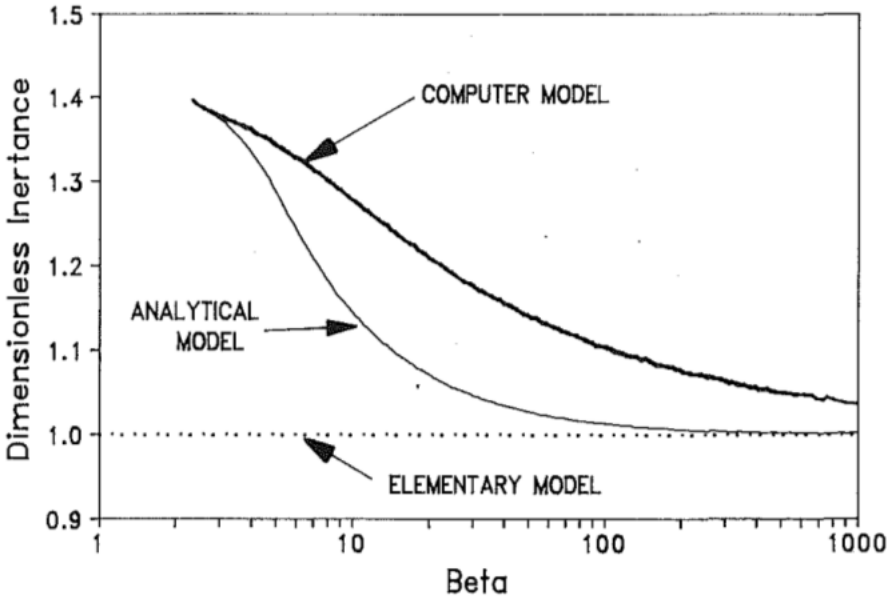

Figure 2.4. Experimental $\frac{\alpha}{\beta}$ vs β [5]

Here again is seen a net difference between the elementary model and the results extracted from the computer simulation.

Thirdly, the actual inertance I is extracted thanks to:

$$I = \frac{\rho l}{\pi r_0^2} \, I_0 \tag{2.24}$$

2.2.2 Results

Let's now have a look at the consequences of this modification.

First a resistance model is to be chosen, depending on the value of α that is used.

In what follows, the following values for r_0 can be expected:

$r_0 = a_0 = 0.828$ mm, inner diameter of all the tubes provided by the manufacturer,

$\nu = 10^{-6}\ m^2/s$ at room temperature.

Given these parameters, the second model is clearly the one to be selected. There-

fore the frequency is comprised between:

$$10 < \alpha < 1000$$
$$\Leftrightarrow 10 < r_0\sqrt{\frac{\omega}{\nu}} < 1000$$

$$\Leftrightarrow 23Hz < f < 2.3\ 10^5 Hz \tag{2.25}$$

This range fits the one needed to the perform the F^{2}MC experiments. Based on the data available [5], a direct correspondence between the frequency and the inertance is quantified. Fitting the raw data gives (see Figure 2.5):

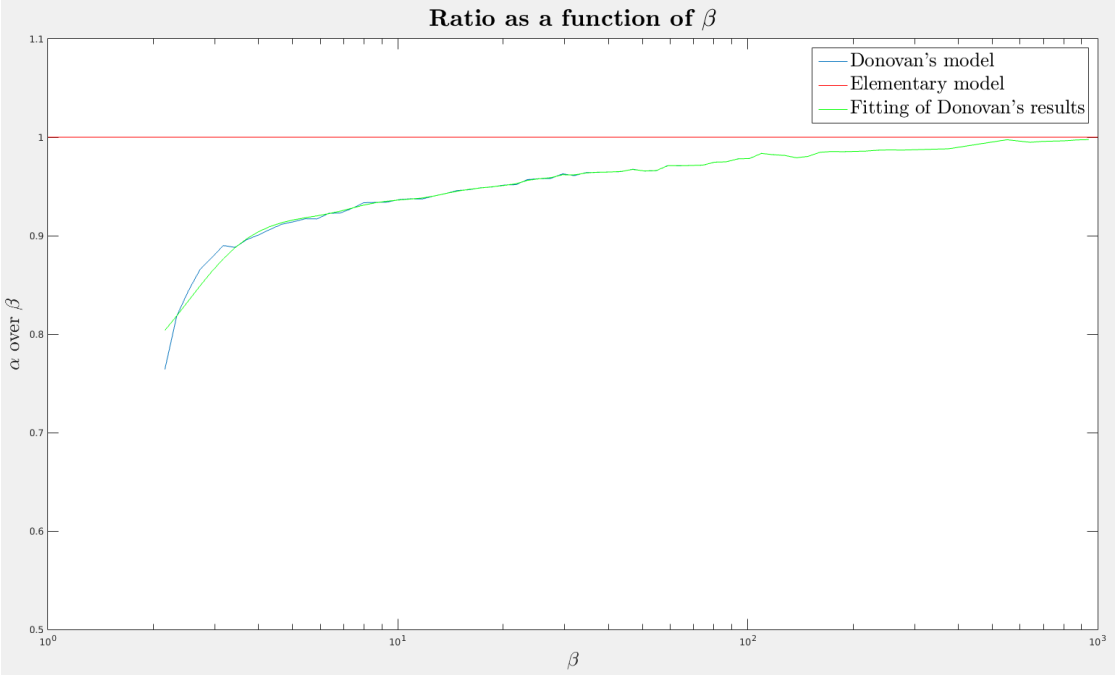

Figure 2.5. Curve fitting for the α/β relationship

Then, the value of the inertance is expressed as a function of the frequency.

The inertance is slightly higher than what was expected previously.

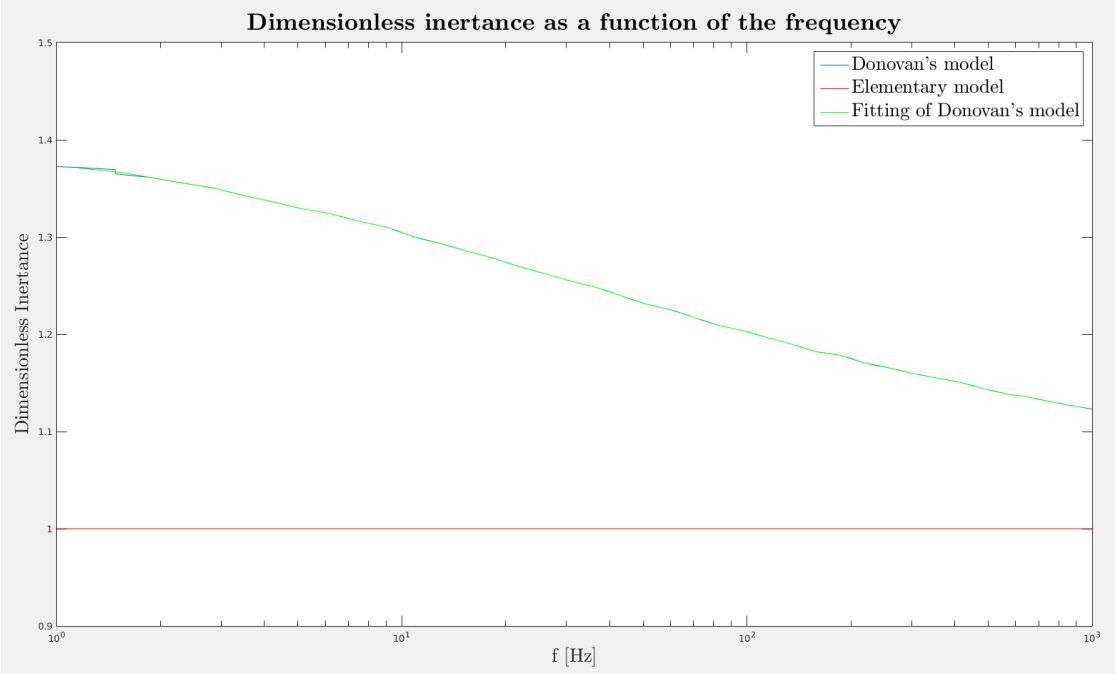

Figure 2.6. New inertance in comparison to the previous model

The resistance found in the new model changes too in comparison to the previous one.

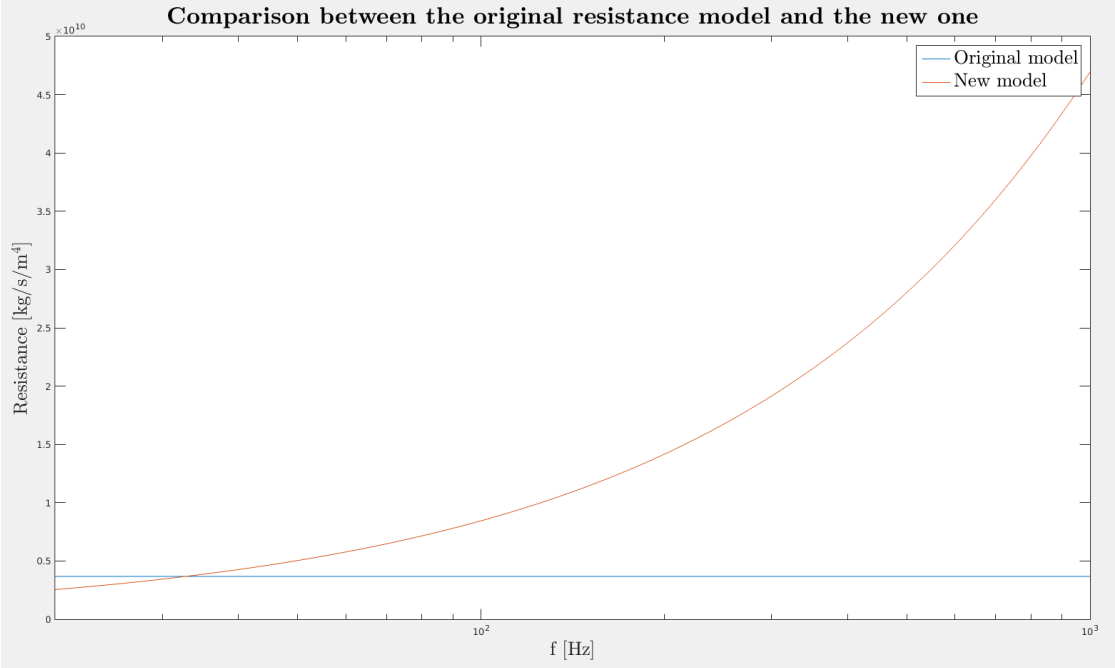

Figure 2.7. New resistance in comparison to the previous model

At low frequency, the initial model and the corrected one are quite close. But as expected, when the frequency goes up the resistance goes up for the corrected model but not for the previous one given that it did not take into account the resistance. This is due to the fact that the fluid does not have time to respond to the excitation at high frequency. Therefore, its resistance increases dramatically.

2.3 Monte Carlo simulations of a tube

The next step that was taken was to increase the performance of the code itself. As it was intended to run one simulation at a time, there had been no emphasize on speed. In this part, details on the different ways to speed up such code and make it a valuable research tool by itself will be explained.

Given how non linear the transfer function of the tube is, it is really hard to predict what will be the FRF for a given set of parameters. Consequently, it is really hard to know beforehand what is the best combination of parameters to target a given

frequency. The code was then modified to be able to run millions of simulation and extract the best out of them.

2.3.1 Designing an objective function

First,"better" has to be defined. When running simulations to optimize a system, there is a need a quantity that can make the difference between two configurations. Let's have a look at the following code run (see Figure 2.8):

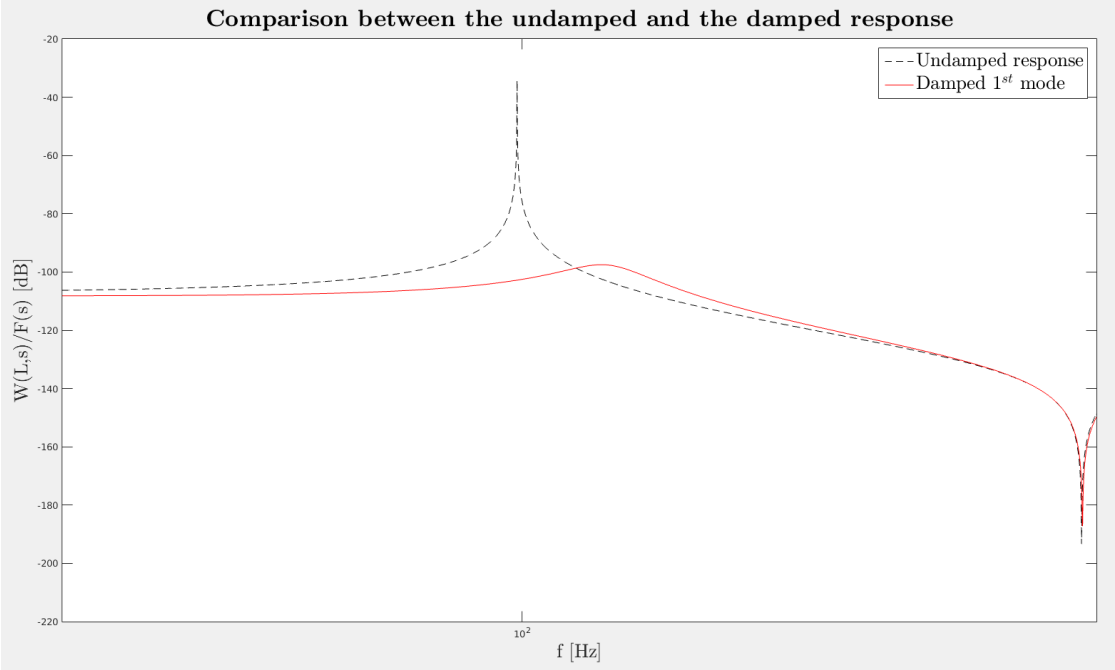

Figure 2.8. Two different runs of the code

In this picture, representing two runs of the same code for different parameters, the red curve looks obviously more promising than the red one. It comes from the fact that the red one evolves in areas of lower transmitivity, which is of interest. Therefore the results will be sorted based on:

$$S = \frac{1}{f_2 - f_1} \left| \int_{f_1}^{f_2} \frac{W(L,s)}{F(s)} \right| df \tag{2.26}$$

This quantity is then called the Normalized Damping (N.D.).
One last thing worth noting is that the Y axis is logarithmic, therefore a small decrease in damping performance somewhere can yield drastically different results when comparing two curves.

2.3.2 Accelerating the code

2.3.2.1 Parallel computing

Matlab now supports the possibility of multicore computing. Up to 512 cores, called "workers" can be used concurrently for high performance applications, provided that they are all on the same machine. Even if without a local supercomputer, most of the commercial grade computers are now shipped with multi-core CPU that can speed up the computations if used the proper way. Matlab does not support logical CPU units, meaning that only physical cores can be used to run parallel code. For instance, while most of the Intel™ Core® i7 have four physical cores yielding eight logical computing units, only one of the two threads per CPU can be used[3] during computation. Therefore, Matlab will detect only four computational units.

Once activated, computations are mostly sped up by the use of the "parfor" instruction replacing the usual "for" one. This tells Matlab to automatically send the work related to the next loop index to an idle CPU until all the work has been performed and returned.

[3]this is done to avoid overlaps when collecting data from different threads

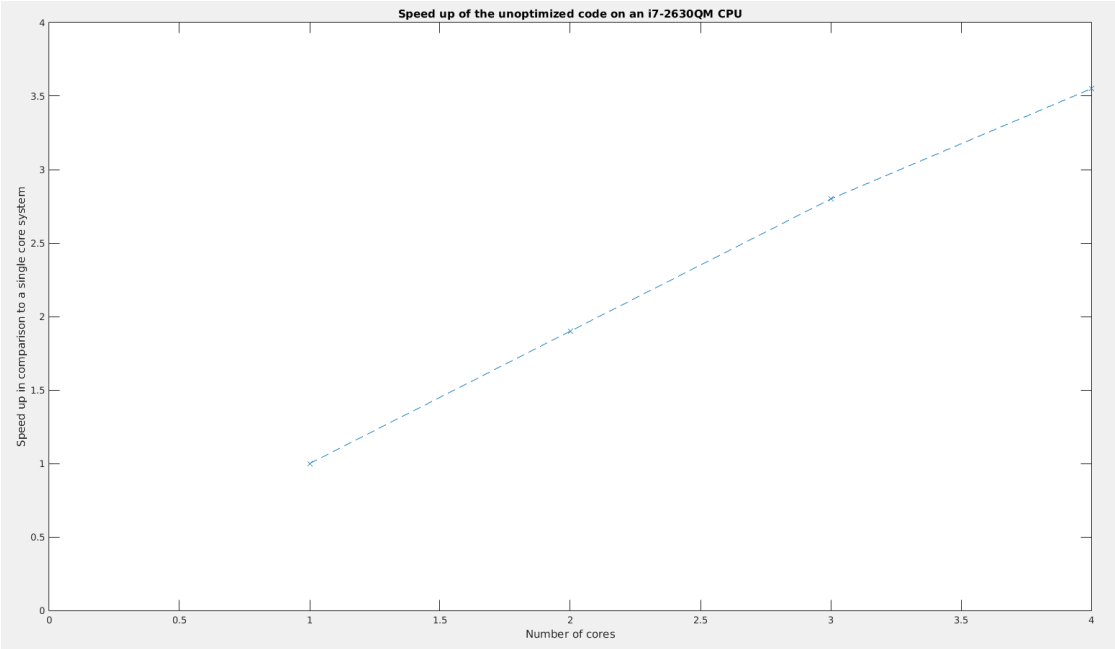

Figure 2.9. Speed up obtained by the use of a parfor loop instead of a for one

This gives us an almost linear increase in performance depending on number of cores on the machine. An order of magnitude in computational speed can be achieved on a recent desktop machine. However, one will have to redesign the code to satisfy the requirement of the Matlab "parfor". The philosophy is quite different while writing a code for multi-core application. Workers cannot access each other's variables and should not modify variables that will be reused by others later [4]. Indeed, given that it is impossible to predict the order in which workers will go through the indexes of the for loop, each write operation has to be carefully watched so that the result of a computation does not depend on which worked wrote some data first.

[4]This is called a "data race"

2.3.2.2 Sparse matrices algebra

The next step that was taken to increase the number of runs per second was to switch to sparse algebra instead of conventional algebra. The characteristic matrix of the system grows in size as a function of the square of the number of tube packs : $16(2N+1)^2$ entries for N packs of tubes. However, a look at the matrix shows that the bigger it gets, the higher the proportion of 0's in it.

Case N = 1:

Line number	Number of zeros per line
1 & 2	10
3 $\sim$ 10	4
11 & 12	8

Table 2.1. Sparse matrice case N=1

Case N = 2:

Line number	Number of zeros per line
1 & 2	18
3 $\sim$ 18	12
19 & 20	16

Table 2.2. Sparse matrice case N=2

General case:

Therefore in the general case there are 16N+3 non zero elements. As a consequence, using sparse algebra allow us to switch from an algorithm dealing with a $O(N^2)$ elements to a O(N), which is a tremendous improvement in speed.

Line number	Number of zeros per line
1 & 2	4(2N+1)-2
3 $\sim$ 4(2N+1)-3	4(2N+1)-8
4(2N+1)-1 & 4(2N+1)	4(2N+1)-4

Table 2.3. Sparse matrice general case

2.3.2.3 GPU computing

In recent years there has been a rise in the number of system using Graphical Processing Units (GPU) to perform massively parallel computations. The reason is pretty simple: GPU are use a high number of small cores able to deal with a reduced set of mathematical operations. If some of these operations are suitable for a simulation, the increase in speed can be really high provided that the code is efficiently parallelized. Through the Parallel computing toolbox Matlab now allows the user to perform some operations on the GPU, granted that there is a dedicated one the local machine[5].

However, current cheap GPU are not faster than cheap CPU: only the high end cards will show a real performance gain over CPUs.

One last thing is of interest mentioning: floating precision. Floating point number can be of single or double precision. Here a really high accuracy is not always needed, so downgrading the code to single precision accuracy could accelerate the computation without loosing too much information. However, given that the default setting is most of the time double precision in consumer systems only professional grade cards will support this feature and accelerate the code.

[5]On chip GPUs like the Intel X000 are not supported. The improvement would be really modest, if any

2.3.2.4 Further optimizations

A few "tricks" can complete the list of modifications that have already been operated on the main code in order to make the code faster.

First, the number of frequency points that are computed can be reduced. The FRF is mostly quite flat across the frequency spectrum. Therefore applying a normal distribution of points to compute centred on the resonance frequency of the undamped system reduces by a lot the number of points to compute. Here is an example centred around the first mode.

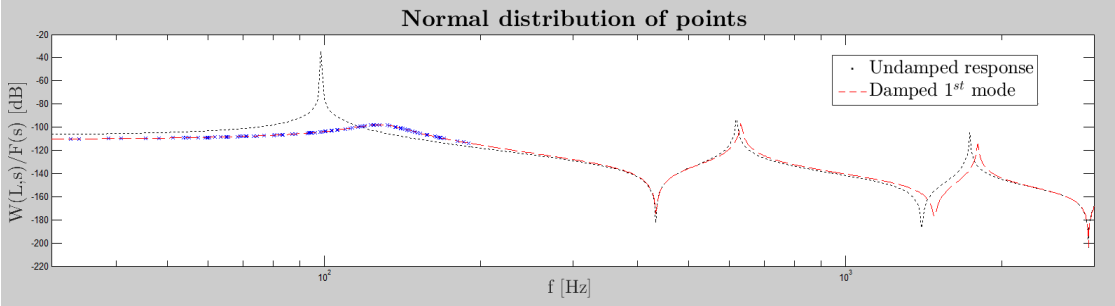

Figure 2.10. Normal distribution of points to compute

The loss in resolution is negligible in regard to the 10 fold reduction in the number of points that have to be computed. The rest is extrapolated based on these points.

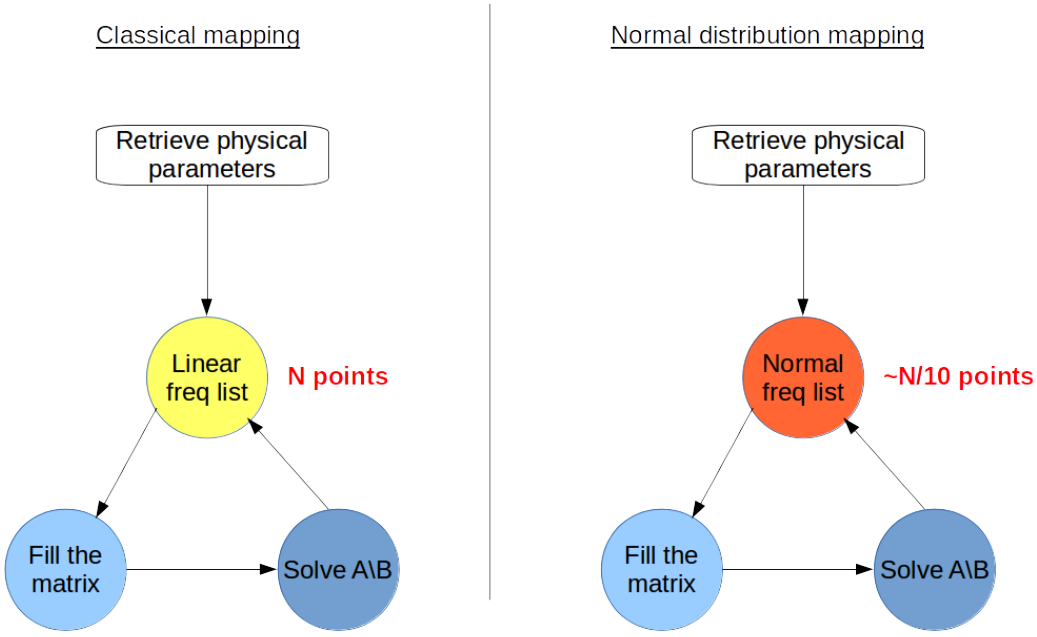

Figure 2.11. Linear and normal frequency mapping

The processes are quite similar, with the distinction in the first second step.

Additionally, instead of inverting one matrix for one frequency at a time, multiple of them can be inverted at once. To do so, a huge block diagonal matrix made of the concatenation of elementary frequency matrices is created. Then, the whole thing is solved and the frequency points of interest are collected.

2.3.2.5 What is the fastest way to run the code?

Two benchmarks give some insights. The first one compared to time needed to invert a given number of matrices depending on how the problem was solved. Five different methods were investigated: CPU with double precision and sparse algebra, CPU with double precision on a full matrix, CPU with single precision on a

full matrix, GPU with a double precision and a full matrix and GPU with single precision and a full matrix.

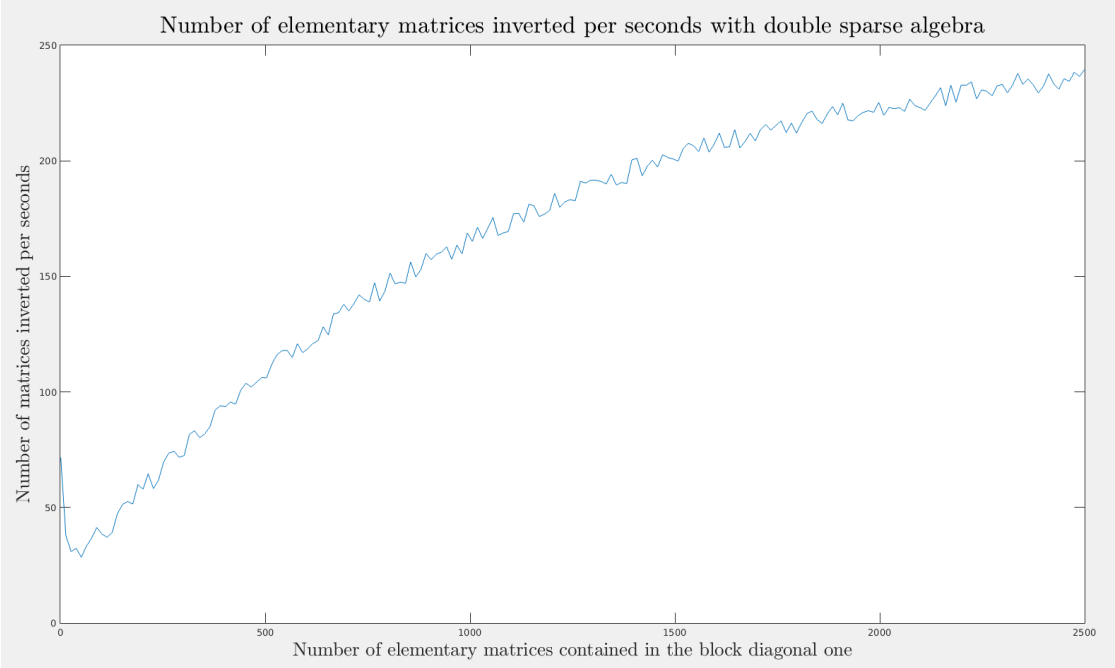

Figure 2.12. Time needed to invert a given number of matrices depending on the method

The imprecision comes from the fact that the system is running other processes than just Matlab at a time. However it is clear that computing on the CPU and using sparse algebra is definitely the way to go. With a more powerful GPU than the one used here, things would probably have been different. Overall the way to go seems to be to use sparse algebra.

Therefore, more work was done on sparse algebra methods and it was found that increasing the size of the block diagonal matrix would at some point not increase the number of elementary matrices inverted per seconds. This is likely to be due to reaching the optimal work repartition among workers and an increase in the time needed to fill the matrix before actually inverting it.

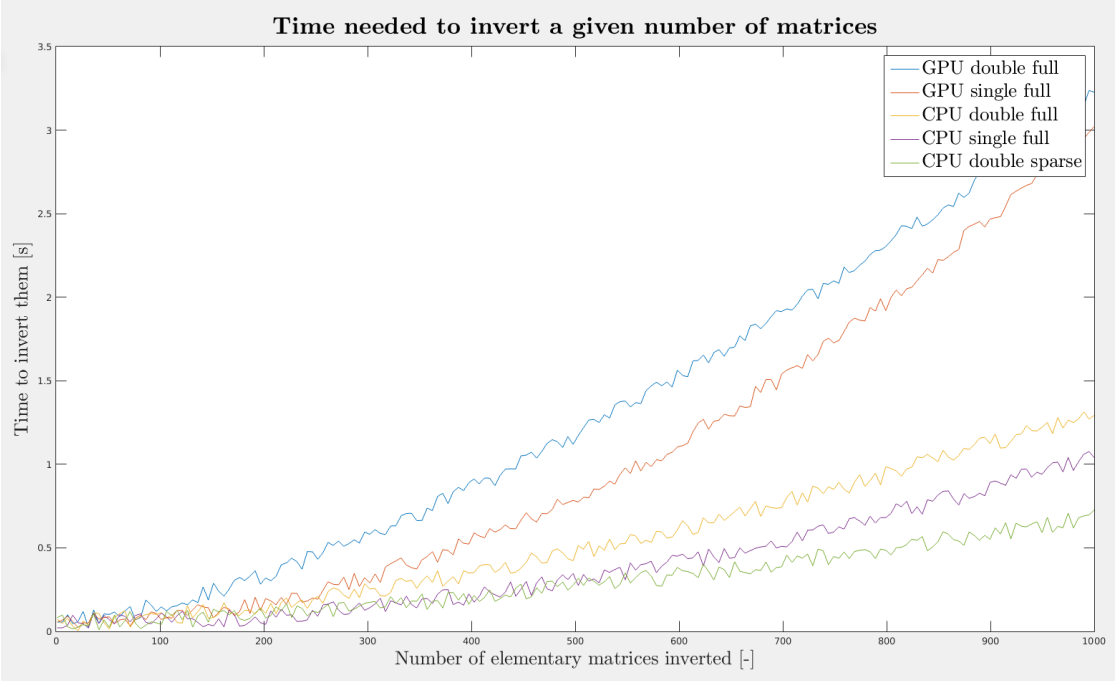

Figure 2.13. Number of elementary matrices inverted per second as a function of the size of the block diagonal one

Therefore a 2000 by 2000 block diagonal matrix was found to be the optimum.

2.3.3 Results of the batch runs

2.3.3.1 Sensitivity analysis

A large amount of simulations was run in order to find a relationship between the input parameters and the total vibrational energy with by a two tubes system. Six parameters were studied, with 10 values for each (leading to a million simulations):

- 1) x_1, position of the beginning of the first tube,
- 2) x_2, position of the end of the second tube,
- 3) y_1, position of the beginning of the first tube,
- 4) y_2, position of the end of the second tube,
- 5) C_d capacitance of the tubes,
- 6) angle of the tube fibres.

The first mode was targeted on a 30 cm long cantilever beam. On the x axis, the value of the parameter can be read. On the y axis is the Normalized Damping. The lower, the better.

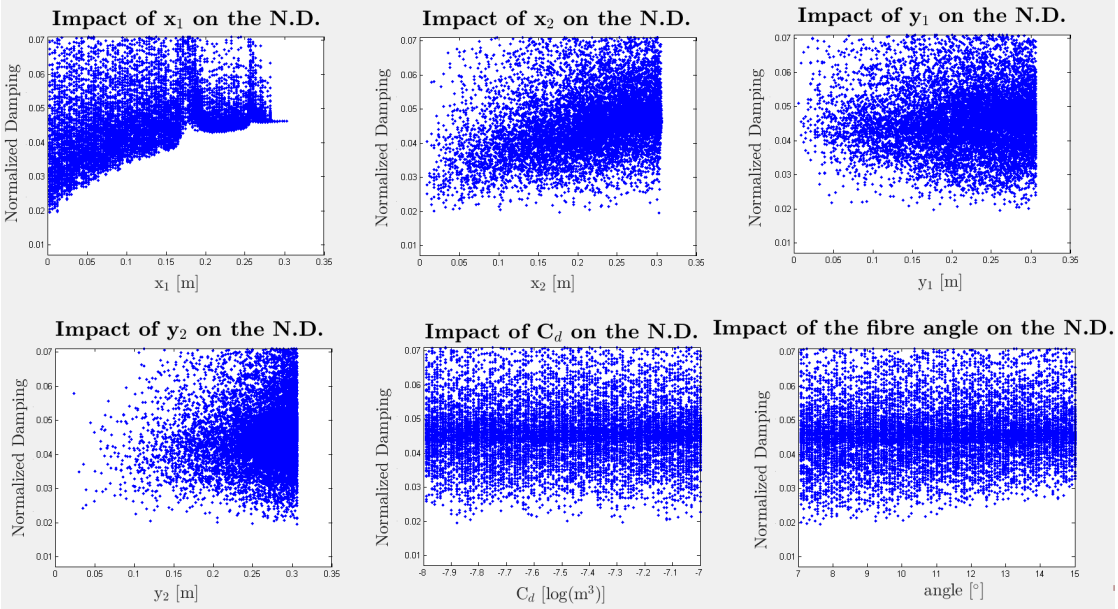

Figure 2.14. Sensitivity analysis for one tube system

A few observations can be made based on these simulations:

i) As Zhu [4] described it, the position of the tubes is directly linked to the mode that is targeted. The maximum slope difference between the beginning and the end of the tubes is desired. Therefore, in the case of targeting the first mode, the best value for x_1 is $x_1 = 0$. Going to higher values reduces the N.D..

ii) For the beginning of the second tube, there is some margin. The best results are uniformly spread. The average N.D. is going up with the distance.

iii) The beginning of the second tube has to be at least 5 mm away from the root of the beam. But other than that, the situation is quite the same as in ii). One distinction is that the average N.D. is not increasing with the distance.

iv) The end of the second tube should be positioned close to the tip of the beam, given that the N.D. slowly goes down with the distance to the root. However this effect is pretty mild.

v) Regarding the capacitance, it's hard to make a conclusion. One point is worth noting though: there is definitely an "average" N.D. here, centred around 0.042. Some results are better, other worse than that but in a pretty symmetrical way.
vi) Lastly, the fibre angle. There is a mix of everything as previously seen. There is an average N.D. around which all the results are plotted, but it is not symmetrical any more. The best results are obtained for a low fibre angle.

Even with millions of simulations, it is pretty hard to formulate a complete theory linking parameters to results. Some results have been found which confirms Zhu's theory, and give additional details on the behaviour of other parameters. The search for an optimal tube was then refined to take these remarks into account and reduce the time spent on a given parameter.

2.3.3.2 Performance optimization

Multiple configurations were studied, to provide a code able to optimize a given frequency with a given amount of tubes. In what follows, the dashed black lines are the FRF of an undamped system, the blue line the FRF of the original parameters and the red lines the FRF of the optmized system. Here are a few screenshots from the code outputs.

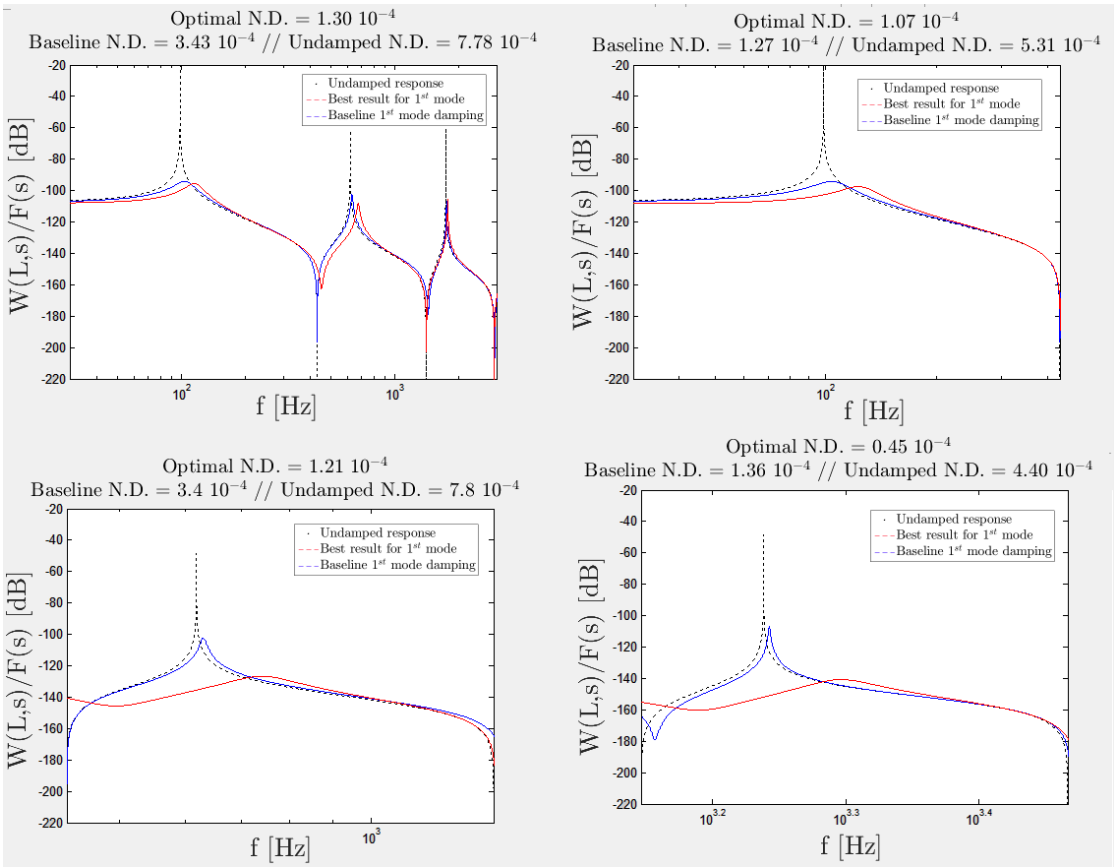

Figure 2.15. Optimization of a given frequency

Here is the optimized one tube system. The top left picture corresponds to an optimization of the system across the first three modes. The top right is an optimization of the first mode, the bottom left an optimization of the second mode and the bottom right an optimization of the third mode. As can be seen some substantial improvements can be made over the initial configuration.

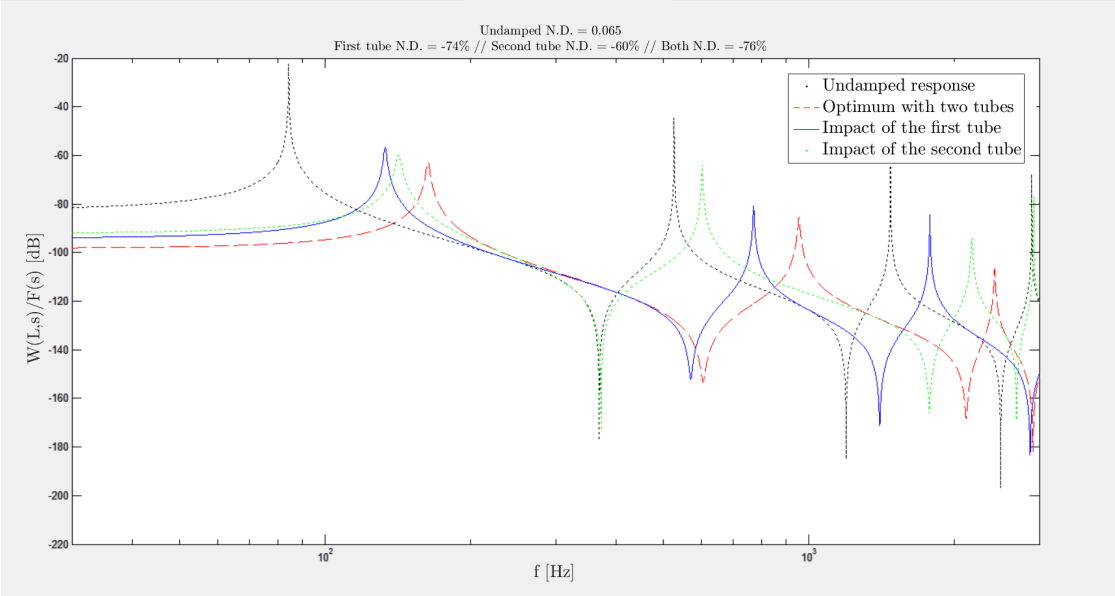

Figure 2.16. Experimental set up related to the previous model [4]

Here is the optimized two tubes system, targeting a frequency span. Even if a one tube system provides good results, it has not been found that two tubes were providing a better damping. This may be due to the reduced set of parameters that were taken into account or the relatively low number of simulations that were performed due to the time needed to perform them. However, it is increasingly difficult to keep the simulation time within reason when exploring new parameters combinations. Unless more powerful hardware is used, it would be difficult to make substantial gains.

Chapter 3
The multi-cell periodic structure

3.1 A new model

Given the good results obtained by the previous work on the F^2MC tubes, a new configuration was investigated. Two categories of tube exist: the "damped absorber" and the "pure damper". The main difference is that the damped absorber has an inertia track at one end, a tube filled with the fluid.

3.1.1 The single-cell model

The damper absorber has promising performances but has one main drawback: in order to get good results, lengthy inertia tracks have to be used. It's obviously not practical.

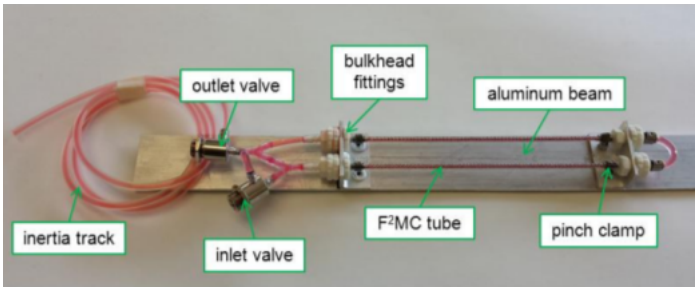

Figure 3.1. A damped absorber configuration mounted on a cantilever beam [4]

Moreover, the tubes can only target one frequency at a time as seen before. They do it really well, but if the frequency that is targeted shifts a little bit, the tube cannot adjust and the vibration level might go up. The need for more flexibility drove us to consider a periodic system.

The main idea was then to put orifices inside the tubes in order to create a mass[1]-spring[2] system that would provide band gaps in the frequency response around a given frequency. The orifices all have the same length in a given tube, and the same inner diameter. Consequently, there is a succession of elementary cells that make up a tube. The fluid is free to move from one cell to another, damping its mechanical energy when passing through the reduced diameter of an orifice.

[1]represented by the fluid
[2]represented by the tube walls

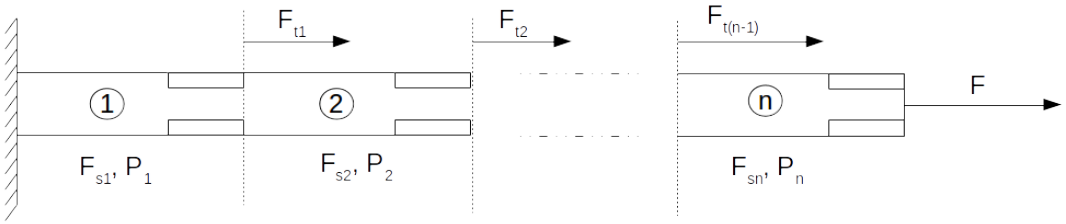

Figure 3.2. Periodic F2MC tube

An analytical model was developed for one cell, two cells, three cells and then N cells. Then, its validity was tested.

Remember the following variables:

$$S_q = -N(\varphi_1 + 2\varphi_2)V_0$$
$$T_q = -N(\varphi_2 + 2\varphi_4)V_0$$

where:

F_{s_1} is the axial force in the fibres

ϵ_k is the displacement for cell k

m is the mass of a cell, m' mass of the last cell plus connectors

I_w is the inertance of the flow Q_{ij} is the fluid flow from cell i to cell j

$S = \pi a_0^2$, section of the tube

where (ϕ_k) are coefficient depending on the geometry and the ply orientation of the tube, extracted from Zhu [4]

Let's now write down the equations needed to solve the system:

$$S_q \mathring{F}_{s_k} + T_q \mathring{P}_k = Q_{k,k+1} \tag{3.1}$$

$$F_{s_k} = F_{t_k} + P_k \pi a_0^2 \tag{3.2}$$

$$\epsilon_k = \phi_1 F_{s_k} + \phi_2 P_k \tag{3.3}$$

$$P_{k+1} - P_k = (I_w s + R) Q_{k,k+1} \tag{3.4}$$

$$F_{t_{k+1}} = F_{t_k} + m' \epsilon_k s^2 \tag{3.5}$$

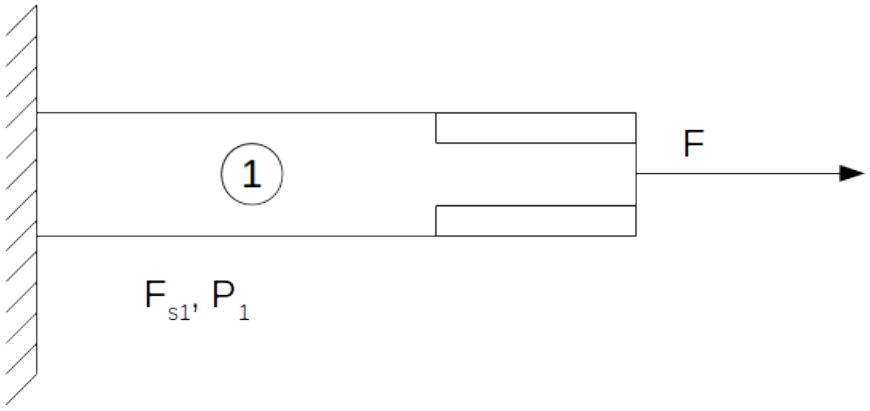

Figure 3.3. Single cell system

Two kinds of equations are present: the fluid flow equations and the force equations.

Fluid flow equations:

$$S_q \mathring{F}_{s1} + T_q \mathring{P}_1 = Q \tag{3.6}$$

$$\Leftrightarrow S_q F_{s1} + T_q P_1 = 0 \tag{3.7}$$

There is only one cell, therefore the flow is zero.

Force equations:

Applying (3.5) comes:

$$F = F_{t_1} + m'\epsilon_1 s^2 \tag{3.8}$$

$$\Leftrightarrow F_{t_1} = F - m'\epsilon_1 s^2$$

Adding (3.2):

$$F - m'\epsilon_1 s^2 = F_{s_1} - P_1 \pi a_0^2 \tag{3.9}$$

Then (3.3):

$$\Leftrightarrow F - m'(\phi_1 F_{s_1} + \phi_2 P_1)s^2 = F_{s_1} - P_k \pi a_0^2 \tag{3.10}$$

$$\Leftrightarrow F = m'(\phi_1 s^2 + 1)F_{s_1} + m'(\phi_2 s^2 - \pi a_0^2)P_1 \tag{3.11}$$

Result:

$$\begin{pmatrix} S_q & T_q \\ 1 + \gamma s^2 & \delta s^2 - S \end{pmatrix} \begin{pmatrix} F_{s_1} \\ P_1 \end{pmatrix} = F \begin{pmatrix} 0 \\ 1 \end{pmatrix} \tag{3.12}$$

where:

$\gamma = m'\phi_1$

$\delta = m'\phi_2$

Solving this system leads to the following solution:

$$G_t(s) = \frac{S_q\phi_2 - T_q\phi_1}{(\delta S_q - \gamma T_q)s^2 - (SS_q + T_q)} \tag{3.13}$$

The numerator has degree 0 while the denominator has degree 2 without a degree 1 term. This is related to the shape of an undamped oscillator. Given that the fluid is not flowing, there is no damping from the fluid part. Here is the FRF of a single cell tube (see Figure 3.4):

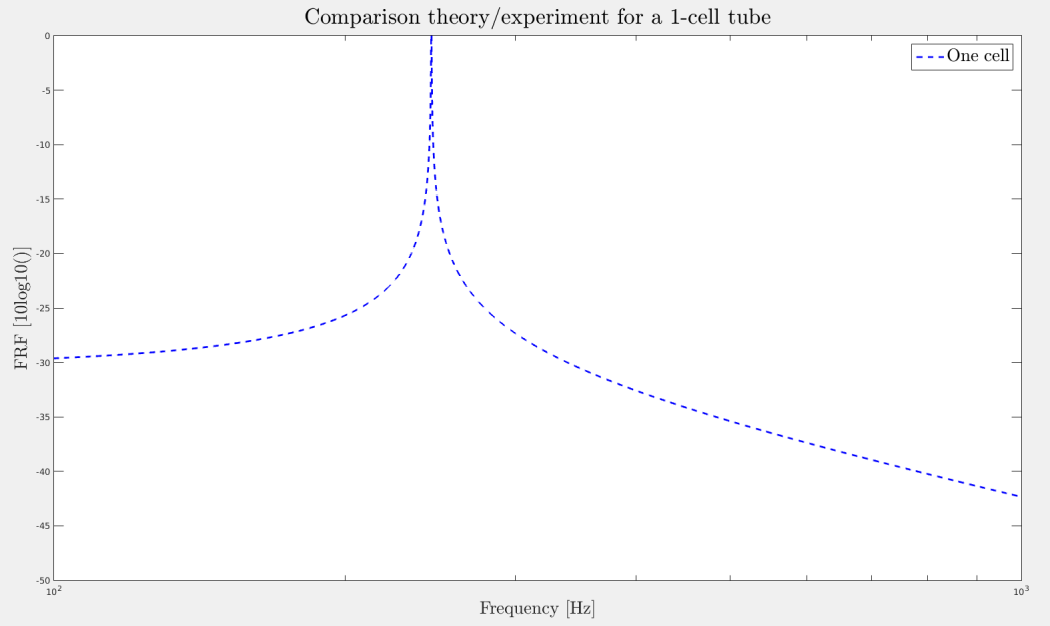

Figure 3.4. FRF of a single tube

3.1.2 The dual-cell model

Let's now extend the model to a tube consisting of two cells.

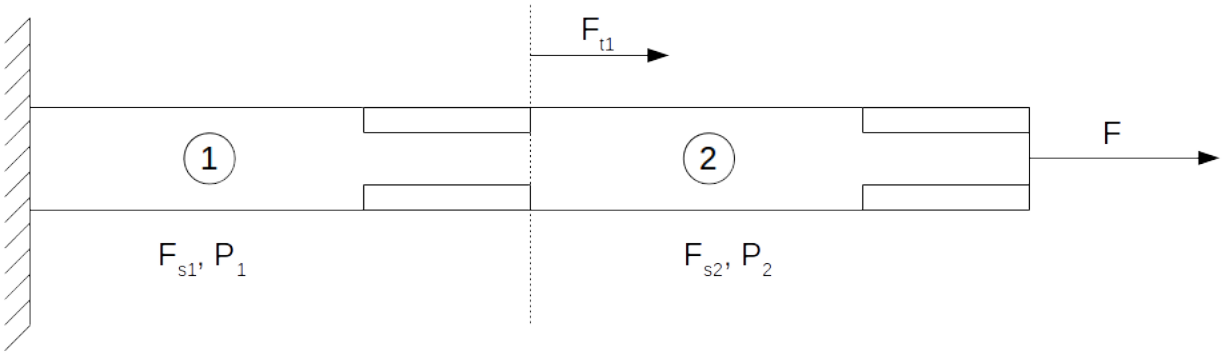

Figure 3.5. Dual cell system

Fluid flow equations:

$$\Delta\mathring{V}_1 = -Q_{1,2} \tag{3.14}$$

$$\Delta\mathring{V}_2 = Q_{1,2} \tag{3.15}$$

Therefore $Q_{1,2} > 0 \rightarrow \Delta\mathring{V}_1 < 0$ as the volume is decreasing.
Consequently:

$$Q_{1,2} = s(S_q F_{s1} + T_q P_1) \tag{3.16}$$

$$Q_{1,2} = -s(S_q F_{s2} + T_q P_2) \tag{3.17}$$

Let's now add the pressure difference equation:

$$P_1 - P_2 = (I_w s + R)Q_{1,2} \tag{3.18}$$

Force equations:
Thanks to (3.5):

$$F = F_{t_2} + m'\epsilon_2 s^2 \tag{3.19}$$

$$\begin{aligned}
&\Leftrightarrow F = F_{t_2} + m'\epsilon_2 s^2 \\
&\Leftrightarrow F = F_{t_2} + m'(\phi_2 F_{s_2} + \phi_2 P_2)s^2 \\
&\Leftrightarrow F = F_{t_1} + m(\phi_1 F_{s_1} + \phi_2 P_1)s^2) + m'(\phi_3 F_{s_2} + \phi_2 P_2)s^2 \\
&\Leftrightarrow F = (1+\gamma s^2)F_{s_1} + (\delta s^2 - S)P_1 + \delta' s^2 F_{s_2} + \delta' s^2 P_2
\end{aligned}$$

Result:

Five unknowns are presents in the system: $F_{s_1},\ P_1,\ Q_{1,2},\ F_{s_2}$ and P_2.

$$\begin{pmatrix} -S_q s & -T_q s & 1 & 0 & 0 \\ 0 & 0 & 1 & S_q s & T_q s \\ 0 & 1 & -(I_w s + R) & 0 & -1 \\ 0 & 0 & 0 & 1+\gamma' s^2 & \delta' s^2 - S \\ 1+\gamma s^2 & \delta s^2 - S & 0 & \gamma' s^2 & \delta' s^2 \end{pmatrix} \begin{pmatrix} F_{s_1} \\ P_1 \\ Q_{1,2} \\ F_{s_2} \\ P_2 \end{pmatrix} = F \begin{pmatrix} 0 \\ 0 \\ 0 \\ 1 \\ 1 \end{pmatrix} \tag{3.20}$$

As before, the equations are solved for $F_{s_1},\ P_1,\ F_{s_2}$ and P_2 so that access to ϵ_1 and ϵ_2 is obtained. Then the expression of the transfer function can be written. The analytical solution starts to be really long. The expression can be found in Appendix A.

Here are one pole and two zeros instead of just one pole.

3.1.3 The three-cells model

Let's detail this last case to show what happens when a cell can have its liquid flow both ways.

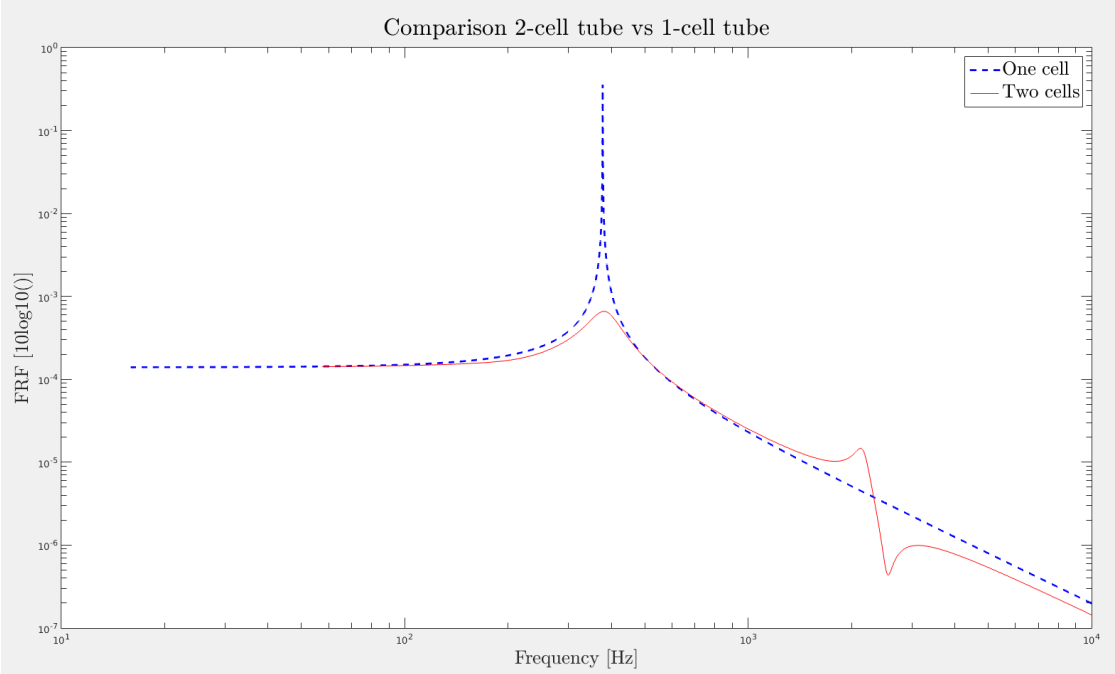

Figure 3.6. FRF of a two tubes system

Fluid flow equations:

$$Q_{1,2} = s(S_q F_{s_1} + T_q P_1)$$
$$Q_{2,3} = s(S_q F_{s_2} + T_q P_2)$$
$$Q_{3,4} = s(S_q F_{s_3} + T_q P_3)$$

Given that a volume change in a cell is equally applied as a pressure on the right and left side the flow can be written as:

$$Q_{1,2} = -Q_{2,3}$$
$$Q_{2,3} = -Q_{3,4}$$

Consequently:

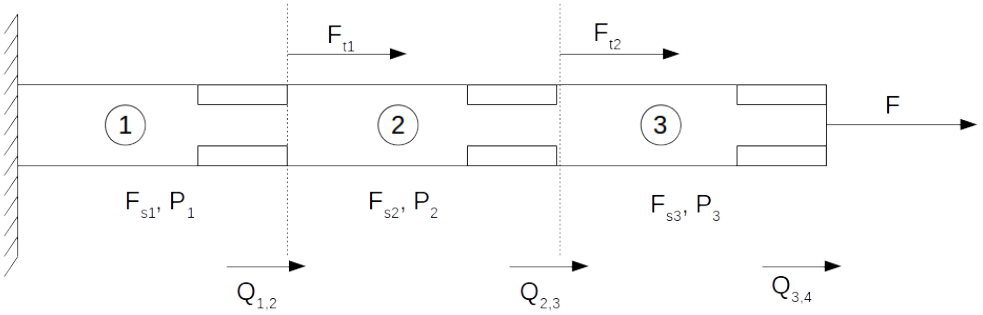

Figure 3.7. Three cells system

$$Q_{1,2} = sS_q(F_{s1} - F_{s2}) + T_q s(P_1 - P_2)$$
$$Q_{1,2} = sS_q(F_{s2} - F_{s2}) + T_q s(P_1 - P_2)$$
$$Q_{1,2} + Q_{2,3} = 0$$

Let's now add the pressure difference equation:

$$P_1 - P_2 = (I_w s + R)Q_{1,2}$$
$$P_2 - P_3 = (I_w s + R)Q_{2,3}$$

Force equations:

$$F_{t_3} = F_{t_2} - m'\epsilon_2 s^2$$
$$F_{t_2} = F_{t_1} - m'\epsilon_1 s^2$$
$$\epsilon_2 = \phi_1 F_{s_2} + \phi_2 P_2$$
$$\epsilon_1 = \phi_1 F_{s_1} + \phi_2 P_1$$

The same procedure as before is applied to get the force equations in their final form.

The result starts to take some place. Mupad processes the result that can then be fed to Matlab to obtain the FRF. See Appendix B for further details.

Result:

$$\begin{pmatrix} -S_q s & -T_q s & 1 & 0 & 0 & 0 & 0 & 0 \\ 0 & 0 & -1 & -S_q s & -T_q s & 1 & 0 & 0 \\ 0 & 0 & 0 & 0 & 0 & 1 & S_q s & T_q s \\ 0 & 1 & -(I_w s + R) & 0 & -1 & 0 & 0 & 0 \\ 0 & 0 & 0 & 0 & 1 & -(I_w s + R) & 0 & -1 \\ 0 & 0 & 0 & 0 & 0 & 0 & 1 + \gamma' s^2 & \delta' s^2 - S \\ 0 & 0 & 0 & 1 + \gamma s^2 & \delta s^2 - S & 0 & \gamma' s^2 & \delta' s^2 \\ 1 + \gamma s^2 & \delta s^2 - S & 0 & \gamma s^2 & \delta s^2 & 0 & \gamma' s^2 & \delta' s^2) \end{pmatrix} \begin{pmatrix} F_{s_1} \\ P_1 \\ Q_{1,2} \\ F_{s_2} \\ P_2 \\ Q_{2,3} \\ F_{s_3} \\ P_3 \end{pmatrix} = F \begin{pmatrix} 0 \\ 0 \\ 0 \\ 0 \\ 0 \\ 1 \\ 1 \\ 1 \end{pmatrix}$$

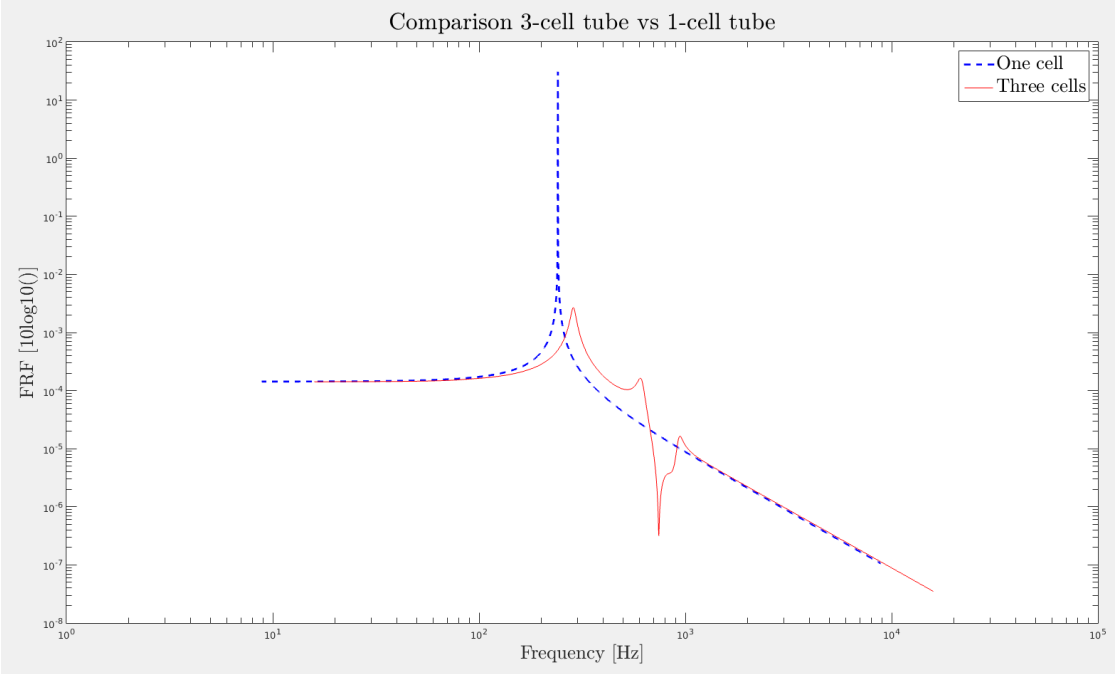

Figure 3.8. FRF of a three tubes system

A wider band gap centred around the resonance frequency starts to be seen. Additionally, a narrow zero is becoming present on the right side of the frequency response. Let's now talk a little bit about the N cells model.

3.1.4 The N-cell model

Deriving a model for N cells follows the same pattern as previously.

Fluid flow equations:

$$\begin{cases} Q_{1,2} = s(S_q F_{s_1} + T_q P_1) \\ Q_{2,3} = s(S_q F_{s_2} + T_q P_2) \\ ... \\ Q_{n-1,n} = s(S_q F_{s_{n-1}} + T_q P_{n-1}) \\ Q_{n,n+1} = s(S_q F_{s_n} + T_q P_n) \end{cases}$$

Let's now add the pressure difference equation:

$$\begin{cases} P_1 - P_2 = (I_w s + R) Q_{1,2} \\ P_2 - P_3 = (I_w s + R) Q_{2,3} \\ ... \\ P_{n-2} - P_{n-1} = (I_w s + R) Q_{n-2,n-1} \\ P_{n-1} - P_n = (I_w s + R) Q_{n-1,n} \end{cases}$$

Force equations:

$$\begin{cases} F_{t_2} = F_{t_1} - m' \epsilon_1 s^2 \\ F_{t_3} = F_{t_2} - m' \epsilon_2 s^2 \\ ... \\ F_{t_{n-1}} = F_{t_{n-2}} - m' \epsilon_{n-2} s^2 \\ F_{t_n} = F_{t_{n-1}} - m' \epsilon_{n-1} s^2 \end{cases}$$

$$\begin{cases} \epsilon_1 = \phi_1 F_{s_1} + \phi_2 P_1 \\ \epsilon_2 = \phi_1 F_{s_2} + \phi_2 P_2 \\ ... \\ \epsilon_{n-1} = \phi_1 F_{s_{n-2}} + \phi_2 P_{n-2} \\ \epsilon_n = \phi_1 F_{s_{n-1}} + \phi_2 P_{n-1} \end{cases}$$

Again, the same procedure as before is applied to get the force equations in their final form.

Result:

$$\begin{pmatrix} -S_q s & -T_q s & 1 & 0 & 0 & 0 & ... & 0 & 0 & 0 & 0 & 0 & 0 \\ 0 & 0 & -1 & -S_q s & -T_q s & 1 & ... & 0 & 0 & 0 & 0 & 0 & 0 \\ 0 & 0 & 0 & 0 & 0 & 0 & ... & 0 & 0 & 0 & 0 & 0 & 0 \\ 0 & 0 & 0 & 0 & 0 & 0 & ... & -1 & S_q s & T_q s & 0 & 0 & 0 \\ 0 & 0 & 0 & 0 & 0 & 0 & ... & 0 & 0 & 0 & 1 & S_q s & T_q s \\ 0 & 1 & -(I_w s + R) & 0 & -1 & 0 & ... & 0 & 0 & 0 & 0 & 0 & 0 \\ 0 & 0 & 0 & 0 & 1 & -(I_w s + R) & ... & 0 & 0 & 0 & 0 & 0 & 0 \\ 0 & 0 & 0 & 0 & 0 & 0 & ... & 0 & 0 & 0 & 0 & 0 & 0 \\ 0 & 0 & 0 & 0 & 0 & 0 & ... & -(I_w s + R) & 0 & -1 & 0 & 0 & 0 \\ 0 & 0 & 0 & 0 & 0 & 0 & ... & 0 & 0 & 1 & -(I_w s + R) & 0 & -1 \\ 0 & 0 & 0 & 0 & 0 & 0 & ... & 0 & 0 & 0 & 0 & 1 + \gamma' s^2 & \delta' s^2 - S \\ 0 & 0 & 0 & 0 & 0 & 0 & ... & 0 & 1 + \gamma s^2 & \delta s^2 - S & 0 & \gamma' s^2 & \delta' s^2 \\ 0 & 0 & 0 & 0 & 0 & 0 & ... & 0 & 0 & 0 & 0 & 0 & 0 \\ 0 & 0 & 0 & 1 + \gamma s^2 & \delta s^2 - S & 0 & ... & 0 & 1 + \gamma s^2 & \delta s^2 - S & 0 & \gamma' s^2 & \delta' s^2 \\ 1 + \gamma s^2 & \delta s^2 - S & 0 & \gamma s^2 & \delta s^2 & 0 & ... & 0 & 1 + \gamma s^2 & \delta s^2 - S & 0 & \gamma' s^2 & \delta' s^2 \end{pmatrix} \begin{pmatrix} F_{s_1} \\ P_1 \\ Q_{1,2} \\ F_{s_2} \\ P_2 \\ Q_{2,3} \\ ... \\ ... \\ ... \\ ... \\ F_{s_{n-1}} \\ P_{n-1} \\ Q_{n-1,n} \\ F_{s_n} \\ P_n \end{pmatrix} = F \begin{pmatrix} 0 \\ 0 \\ 0 \\ 0 \\ 0 \\ ... \\ ... \\ ... \\ ... \\ 1 \\ 1 \\ 1 \\ 1 \\ 1 \end{pmatrix}$$

A general solution to the system of linear equations has not been found. Therefore if one wants to find the analytical solution for a given number of cells, it has to solve it on mupad first before actually using it. However, for $N > 10$, solving the system starts to take hours. Therefore Matlab is used to solve the system numerically.

Generally speaking, more cells will mean more zeros and poles even if some of them are so close to each other that they do not appear. The band gap around the

targeted frequency gets wider even if some additional narrow peaks appear inside.

3.2 Time rate fluid losses of a tube

3.2.1 Bubbles in the tube

After making the tubes, a few tests were performed in order to ensure their physical integrity. However, it soon appeared that the tubes were leaking.

Previous experiments had only used the tubes for a short amount of time: they would be quickly filled with a solution of water and photo film. Any air bubbles that would be present inside the tube would be extracted by gently hitting the tube with the tip of a finger and then the experiment would be run on an open loop circuit. If some bubbles were spotted at any time during the experiment, the option of removing them and refill the reservoir to make up for the water loss was still on the table. Therefore bubble creation was a managed issue.

In the current case, it is a slightly different problem. Indeed, the tubes used are closed at both ends when created. Part of the tube is assembled, fill it and then seal both ends with some epoxy glue. Before sealing the second end, it is important to make sure that no air bubble is present inside. If a bubble appears when the tube is sealed, it has to be discarded given that the absence of bubbles is critical to the experiment and there is no non-destructive way to extract them at that point. Bubbles make the bulk modulus of everything contained in the tube collapse: instead of the usual 2 GPa for the bulk modulus of the water, it can go under the threshold of 400 MPa even with tiny bubble and prevent any damping effect to appear. Therefore, given the characteristic dimensions of the tubes no bubble can exist inside it.

3.2.2 An unexpected leak

However, even after careful filling the tubes, some bubbles were still present in the tube. Here is the latest protocol to fill a tube.

1) Fill a tank of the fluid that will be used to fill the tube

2) Cut a tube from the main lines to the required length[3]

3) Submerge the tube in the liquid to use

4) Using a syringe with a really thin needle, fill the tube

5) Insert a custom made plug at one end of the tube. Plug it in just enough so it will not leak but not all the way

6) Bring the tube out of the liquid

7) Clean the end of the tube to remove any trace of liquid

8) Spread some fast drying epoxy on the end connection and insert the plug all the way in the tube

9) Add a tube clamp to ensure physical integrity during the vibration tests. Epoxy is pretty bad at coping with vibrations for extended period of times.

10) Let the epoxy dry vertically for at least 20 minutes

11) Adjust the liquid level with the syringe

12) Plug in the other end, not all the way

13) Clean the end, add epoxy and then insert all the way the plug. This step ensures some pressurization of the tube given that the water is supposed to be incompressible. Internal pressure helps setting up the fibres in the right direction and have the different layers of the material to pressed one against each other

14) Add the tube clamp while the epoxy is still liquid

15) Let the whole thing dry for a day

Unexpectedly, any single tube made, no matter how well, would have bubbles in it after a day. Multiple drying positions were investigated, multiple glues with

[3] In the range of a few tens of centimetres

different chemical properties[4] were used but the same effect would be observed. The quality of the seal was strongly suspected at first, but after ruling out all the possible factors leading to a leakage, the idea that the tube walls themselves could be leaking emerged. This idea was backed by the fact that a horizontal tube would have bubbles appearing in it in random positions along the length, while if the leaks were due to an incorrect sealing then most of the bubbles would have appeared at the ends and stayed there.

A days long experiment was then run to assess how fast the tube was leaking and find ways to prevent this from happening.

3.2.3 Setting up a leak detection protocol

Volatility is suspected to be the culprit in the bubble apparition. The liquid would evaporate through the walls. Therefore the experiment was run with 4 different fluids have various saturation pressure at room temperature. Additionally, three different thermal environments were used. Here is the composition of the tubes used in each place:

Tube number	Fluid	Comment
1	Oil	Lowest viscosity
2	Water + dye	First water tube
3	Water + dye	Second tube, for redundancy
4	Water + dye	Third tube, for redundancy
5	Isopropyl alcohol	-
6	Nail polish remover	Highest volatility

[4]Silicon, epoxy, vacuum glue...

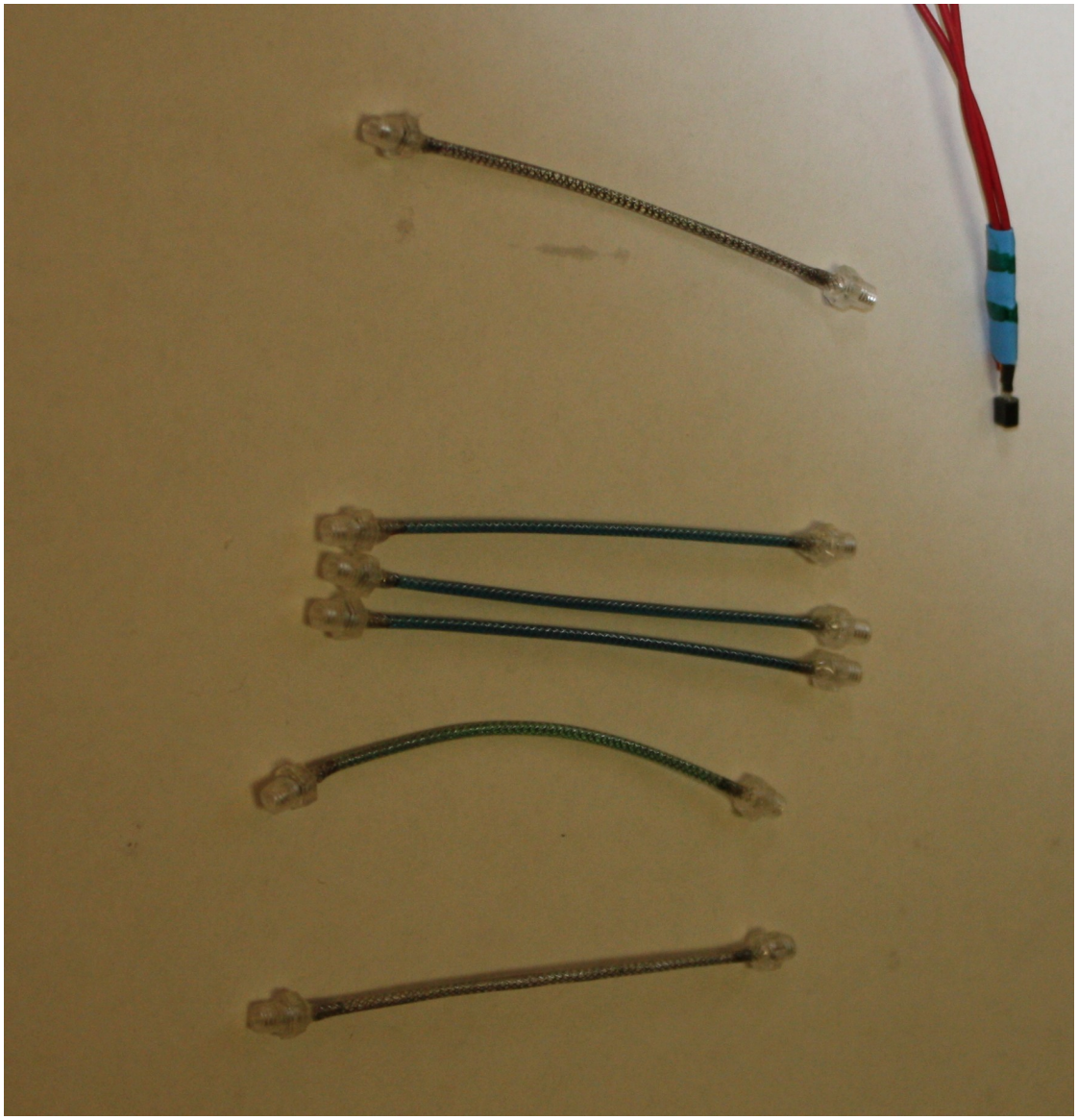

Figure 3.9. Set of tubes to be studied. From the top: oil, water 1/2/3, isopropyl alcohol, nail polish remover. To the right: thermometer

Three sets of six tubes were used. One set was placed in a fridge (low temperature, maintained by the fridge), one in the ambient air (room temperature, maintained by A/C system), one in an oven (high temperature, maintained by the oven). The temperature and humidity was logged in real time by a Raspberry Pi connected to an Arduino equipped with DS18B20 temperature sensors[5] and one

[5]From Maxim integrated

RHT03 humidity sensor[6].

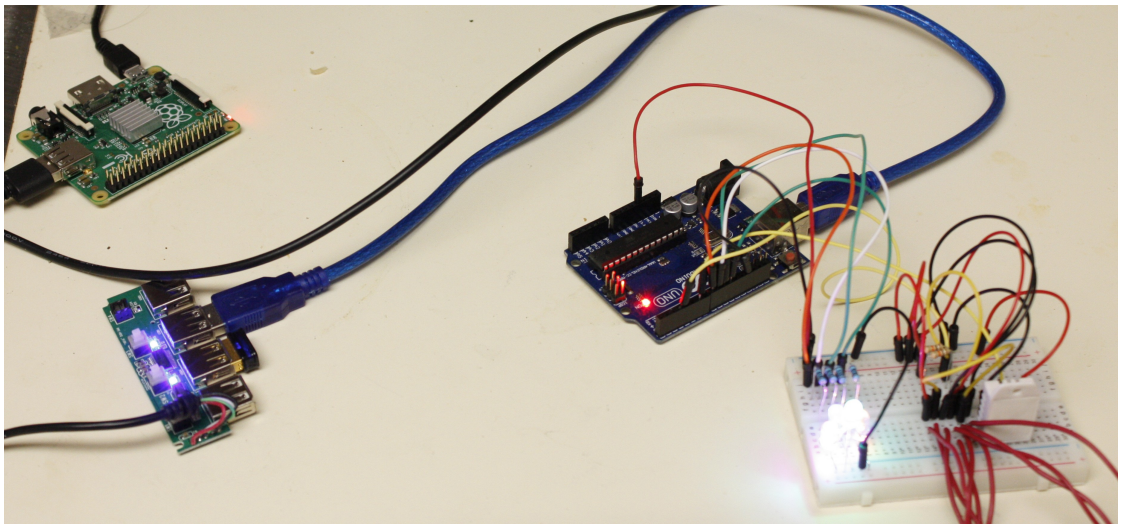

Figure 3.10. Electronic system tracking temperature and humidity

The tubes were made one by one. Given that it takes quite a long time to make a single one, they were introduced one after each other in their respective environment. The time they were introduced was recorded. Introduction of a tube in the fridge or the oven proved to have a negligible impact on the environment temperature as recorded by the sensors.

[6]From MaxDetect

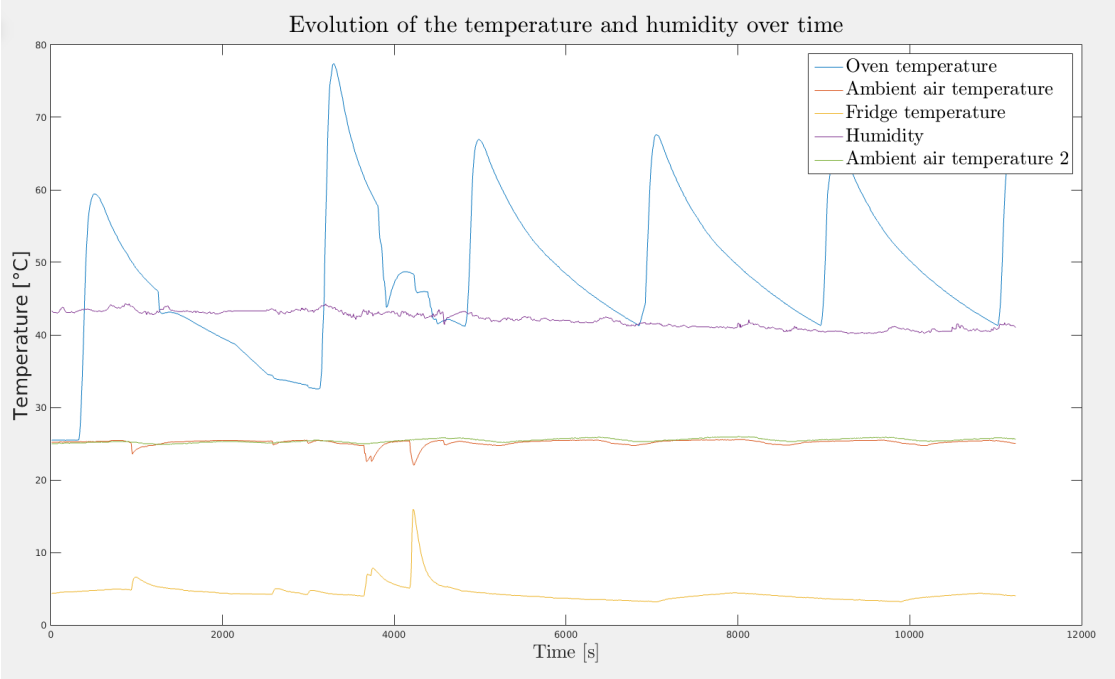

Figure 3.11. Evolution of the temperature and humidity

The temperature and humidity remained pretty much constant in the fridge and in the room. However, it is not the case of the oven. A cheap temperature controller is probably to blame here. Despite a 70°C demand, it would stop working the second it reaches 70°C, progressively loose heat and start to heat again when approximately 40°C where reached. The temperature was assumed to be maintained at an average "55°C".

Every couple of hours, the tubes were extracted from their environment and weighted on an electronic scale with a 0.01 g resolution, at ± 0.01 g of accuracy. Then, the tubes were return to their environment.
After a few days, all the data was collected and loss in liquid over time was plotted for each tube.

3.2.4 Results

3.2.4.1 Fridge

First let's have a look at the evolution of the weight of the tubes that were stored in the fridge. The temperature was constant for three days, around 4.8°C.

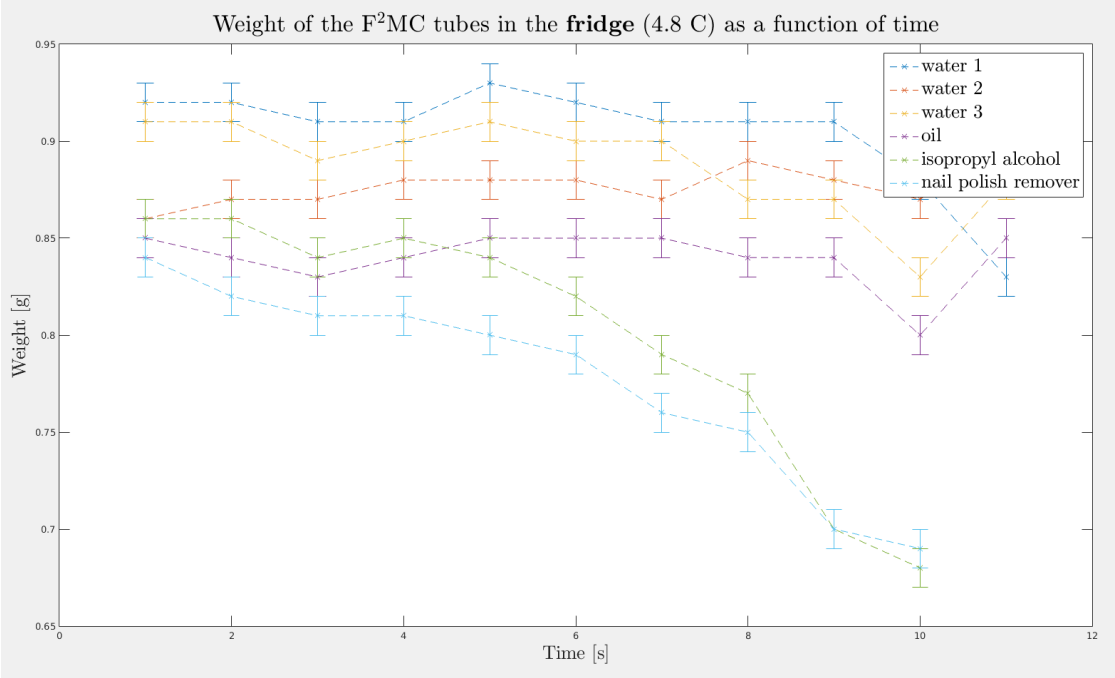

Figure 3.12. Evolution of the weight of the tubes at 4.8°C

After three days in the fridge, the nail polish remover and the isopropyl alcohol have vanished. One tube filled with water is also being depleted at a steady rate. However, two of the water tubes and the oil tube do not look like they have been leaking. This was correlated by an observation of the tubes: one filled with water had tiny bubbles, the one filled with nail polish remover and isopropyl alcohol clearly had air pockets.

3.2.4.2 Ambient air

Secondly, let's consider the tube that stayed outside. The temperature was constant for 3 days, around 25°C.

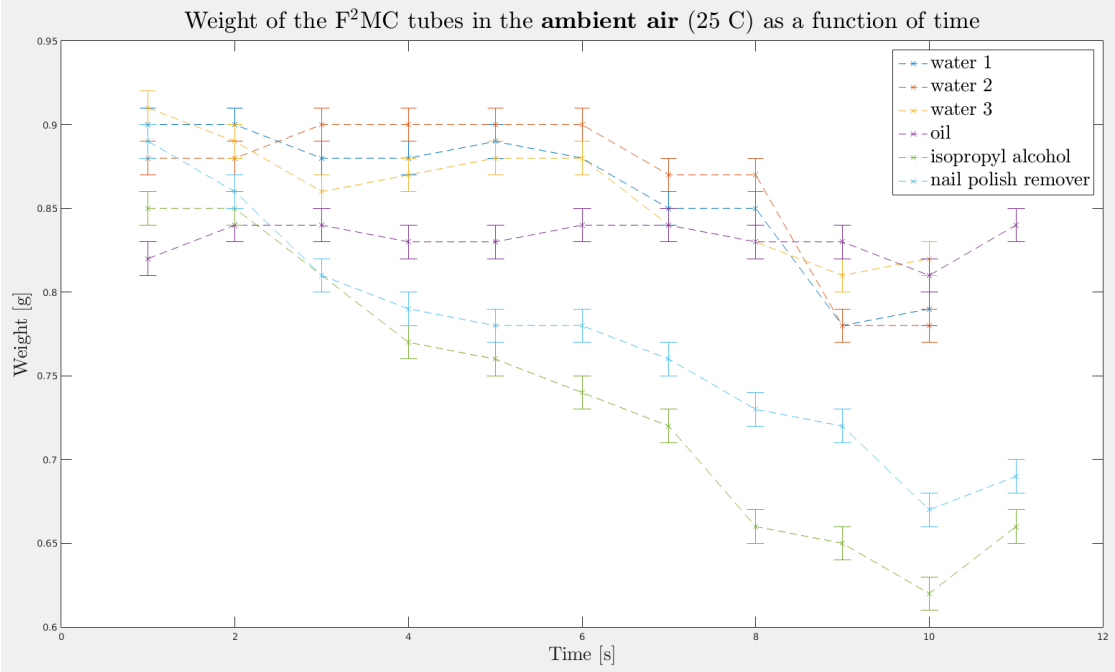

Figure 3.13. Evolution of the weight of the tubes at 25°C

The isopropyl tube and the nail polish remover tube have lost a lot of weight and were depleted at the end of the run. The tubes filled with water all had lost a substantial amount of liquid. The tube filled with oil had no visible bubble, which is supported by a steady weight.

3.2.4.3 Oven

Lastly, let's have a look at the results from the oven. The temperature was not constant, as seen before, but the results are clear (see Figure 3.14):

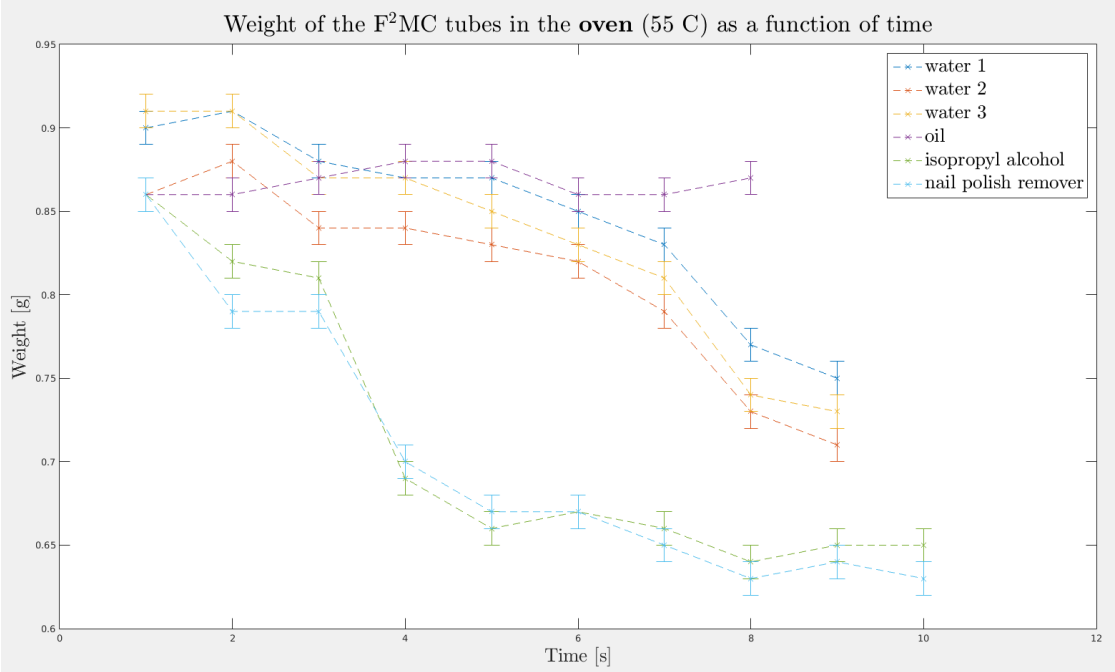

Figure 3.14. Evolution of the weight of the tubes at 55°C

All the tubes are either depleted in liquid or about to after only a day in the oven. Only the tube filled with oil does not have a measurable amount of leaks, which is confirmed by direct observation of the tube.

3.2.5 Conclusion

Given these results, the conclusion is that the walls are porous to liquids. Some leak time rates have been determined for four different liquids. Consequently, as long as some kind of oil is used, there should not be any major leak issue. Performance may be reduced, therefore to limit this a specific oil was chosen, the SPF-1 provided by Lord Corporation. It was specifically developed to offer good performance in fluidic systems, has a low viscosity, a low volatility and a high density ($\rho = 1800$ kg.m^{-3}).

3.3 Test runs

3.3.1 Experimental set-up

An aluminium frame was built on a isolated table to connect the tubes to a shaker. This way, longitudinal vibrations of the tubes can be studied. At first, an accelerometer and a force sensor were used to determine the FRF. Then, an impedance head was used, placed close to the shaker so that acceleration and force were measured at the same place.

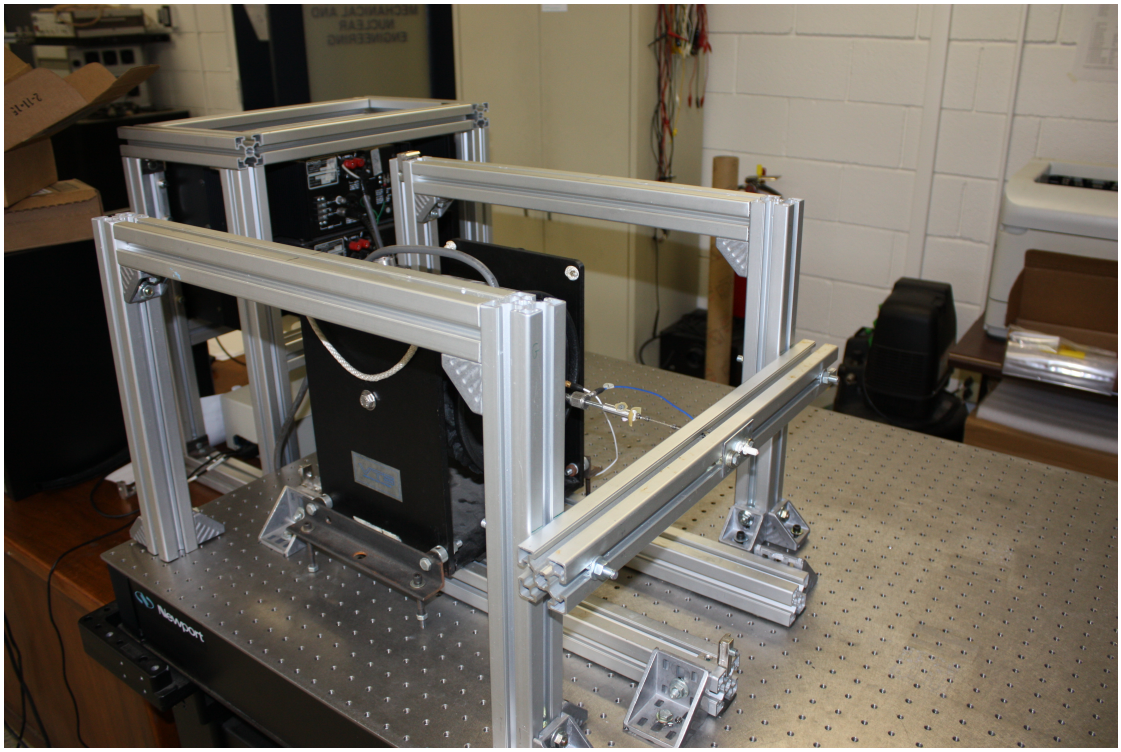

Figure 3.15. Tube in longitudinal vibrations

The connection of the tube with the shaker and the frame have to be exactly in front of each other. Even if this is theoretically impossible, the typical accuracy was around a diameter on the frame end.

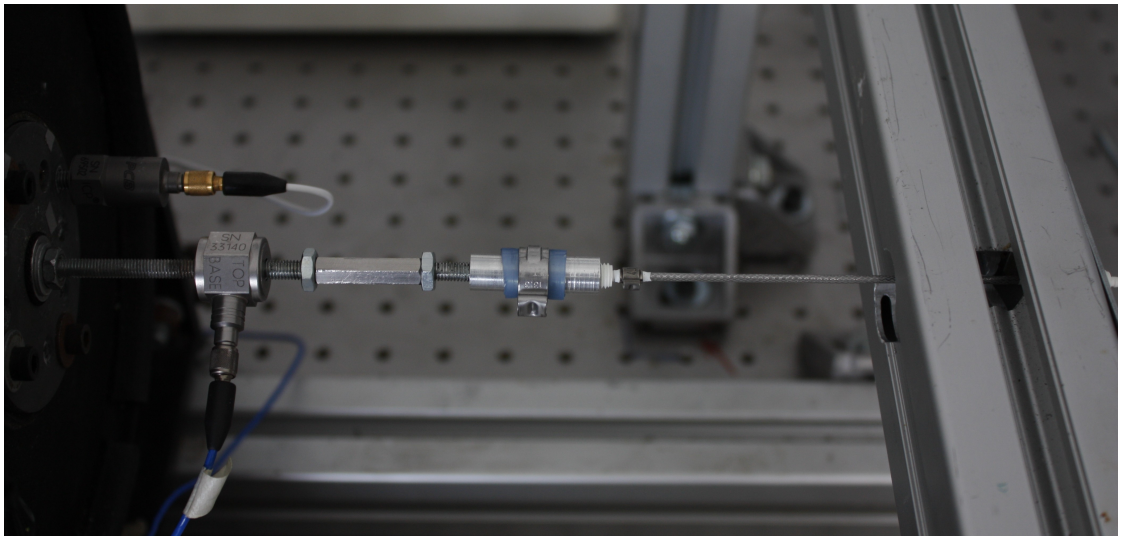

Figure 3.16. Detailed view of the position of the tube

The first few runs showed that the frame was shaking a lot, therefore most of the connections were insulated with rubber washers. An unknown peak was still appearing around 360 Hz. Placing a 31.4 pounds cinder block on the horizontal bar of the frame shifted it to the low frequency end of the spectrum. It's not practical to run the experiments with the cinder block on, so this peak was just identified and linked to the frame in all the following results.

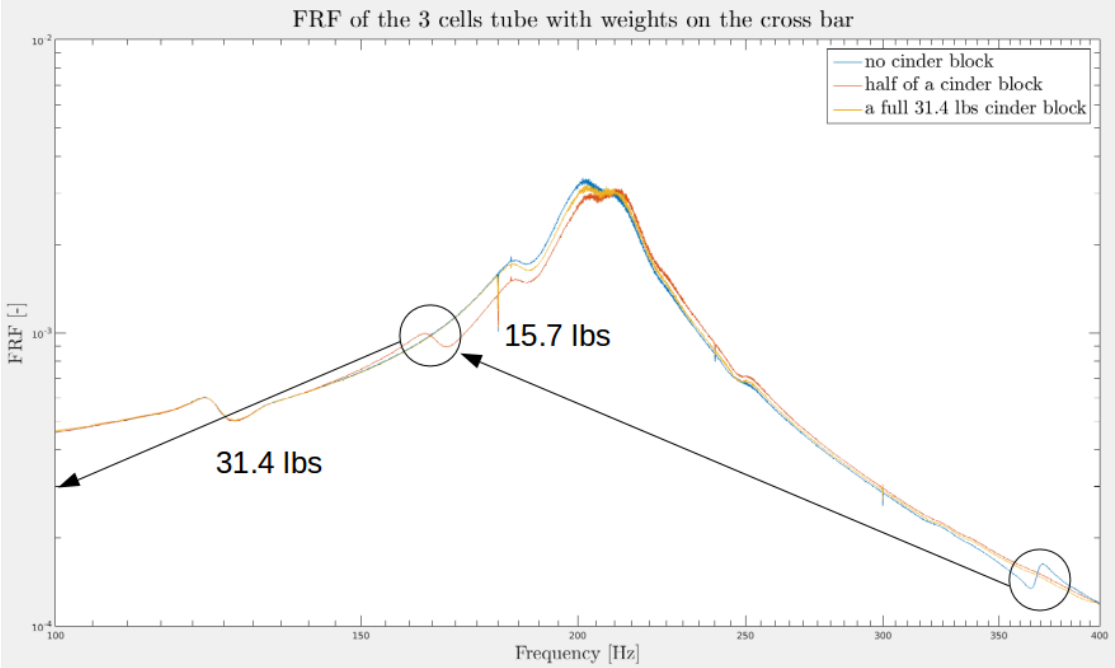

Figure 3.17. Impact of a cinder block on the horizontal bar of the frame

Here it is clear that the 365 Hz peak is moved to 170 Hz when half of the cinder block is added and then to disappears from the FRF.

3.3.2 Static stiffness

3.3.2.1 Tube filled with air

First the static stiffness of a tube filled with air is measured. A 90 cm long tube was hung from a support. Weights were gradually added to the free end of the tube, where the displacement was measured. The following force/displacement response was obtained (see Figure 3.18):

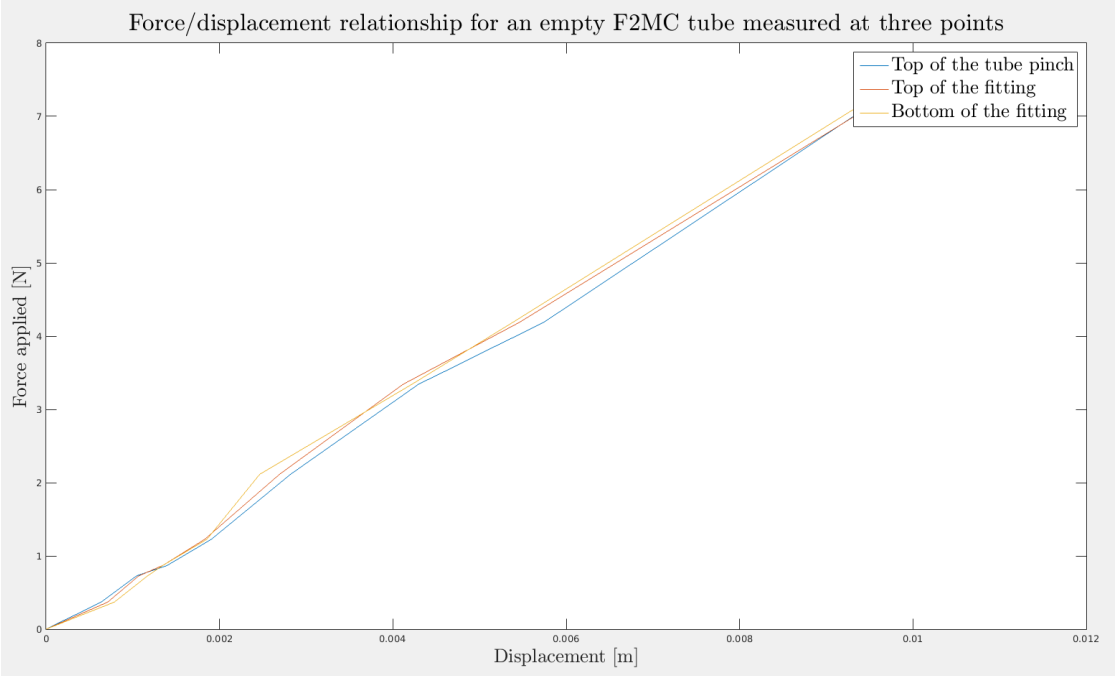

Figure 3.18. Force/displacement relationship for a tube filled with air

The displacement was measured in three different points. The agreement between all of them turned out to be pretty good. The static stiffness of the tube itself can easily be computed.

$$F = k_{air}x \tag{3.21}$$

Here it reaches 764.9 for the tube, therefore:
$k_{air} = 8241N/m$ for a 8.3 cm long tube, which is the format used for the dynamic experiments.

Additionally, the 8.3 cm tube was weighted at $m = 16.16$ g. Consequently:

$$f_{air} = \frac{1}{2\pi}\sqrt{\frac{k_{air}}{m}} \tag{3.22}$$

$$\Leftrightarrow f_{air} = 113.6Hz$$

3.3.2.2 Tube filled with SPF-1

Then is tested a tube filled with SPF-1. The same protocol was followed the same protocol.

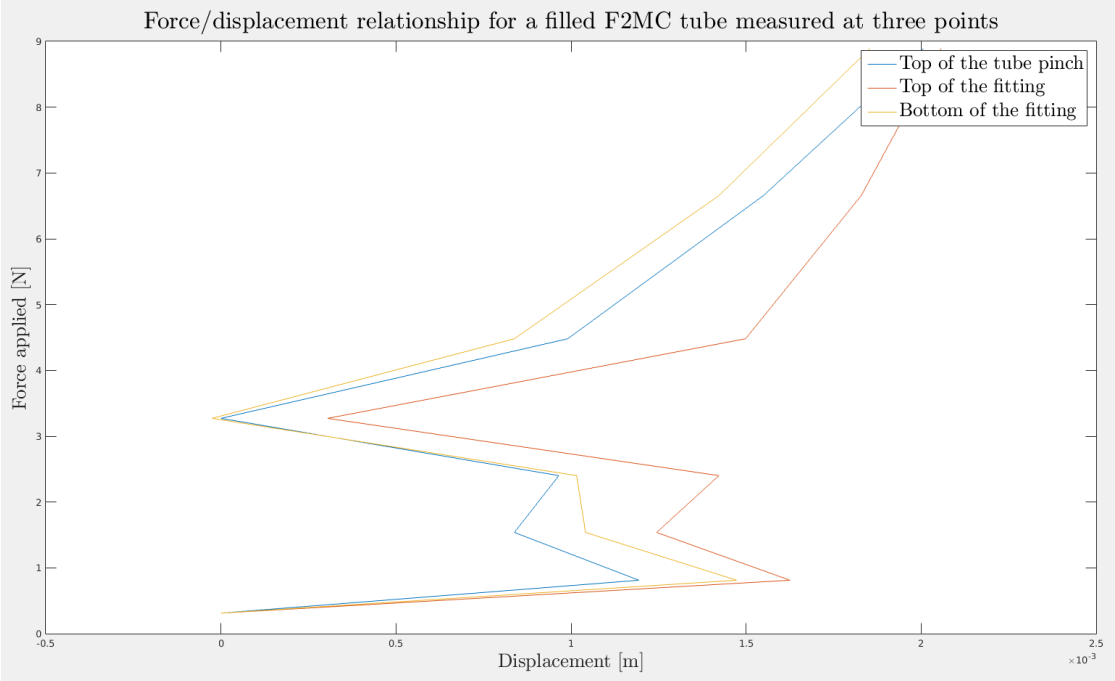

Figure 3.19. Force/displacement relationship for a tube filled with SPF-1

This time, the agreement is lower for low weights. This is probably due to the fact that it takes a bit of weight to have the fibres ready to be under tension given that the fluid is now adding a decent amount of stiffness. However, the force/displacement relationship starts to be linear afterwards.

$$F = k_{air}x$$

Now it is 4305 for the tube.

$k_{air} = 46681 N/m$ for a 8.3 cm long tube, which is the format used for the dynamic experiments.

Additionally, the 8.3 cm tube was weighted at $m = 16.5$ g. Consequently:

$$f_{air} = \frac{1}{2\pi}\sqrt{\frac{k_{air}}{m}}$$
$$\Leftrightarrow f_{air} = 267.7 Hz$$

3.3.3 Details on the frequency sweeps

Most of the tests were run from 100 Hz to 400 Hz, with some of them being extended to up to 1000 Hz. The sensors are sampled by an acquisition box connected to Labview. 100 000 samples are taken per second from the accelerometer and the force sensor, for 10 seconds. It brings a million point for the FRF.
Each FRF is averaged 10 times to reduce the noise. Usually, the noise level is pretty low given the good insulation provided by the table. A high noise level would usually mean that something is loose. However, a peak every 60 Hz can always be seen, due to the electrical current.

3.3.4 Results

3.3.4.1 Tube filled with air

A few tubes just filled with air were tested in order to get the FRF of the tube itself. However, the value of the resonance frequency depended on the pretension that was applied to the tube before running the experiment. Therefore the experiment was run for different pretensions.

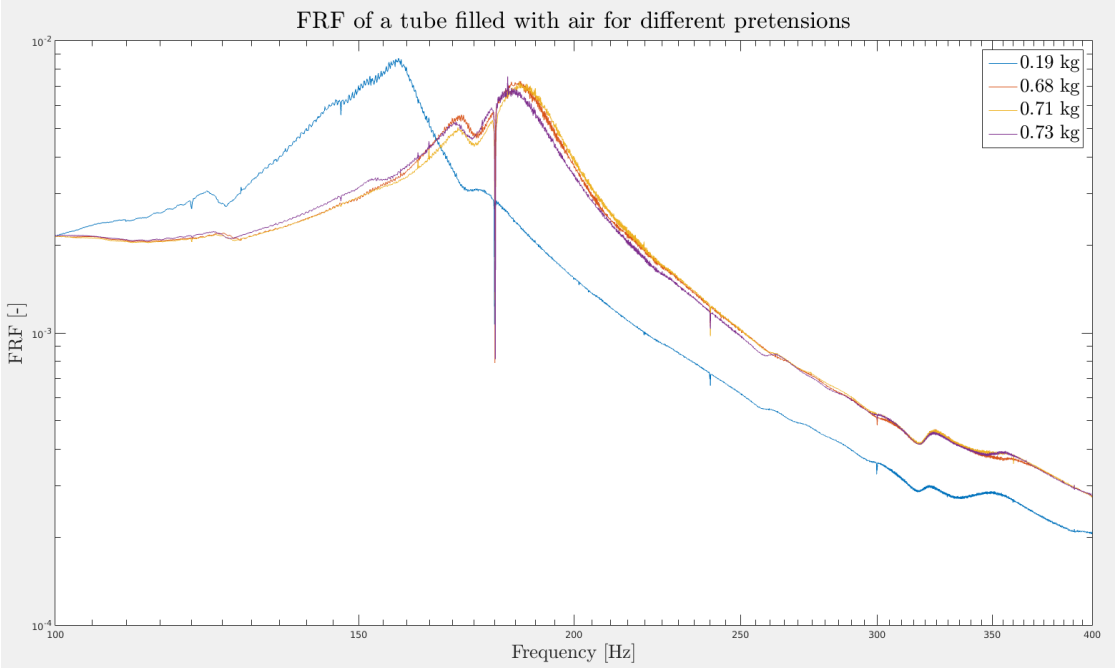

Figure 3.20. FRF of a tube filled with air for different pretensions

Clearly, there is a difference between the runs. Even if the shape remains the same, the resonance frequency is different. A consistent explanation for this variation was not found. In theory, the resonance frequency should be found around 110 Hz, but results seemed a bit higher. Some other modes than just longitudinal might have been excited.

3.3.4.2 Tube filled with SPF-1

Single cell tubes filled with SPF-1 gave pretty much the same shape, even though they were shifted to the right due to their increased stiffness.

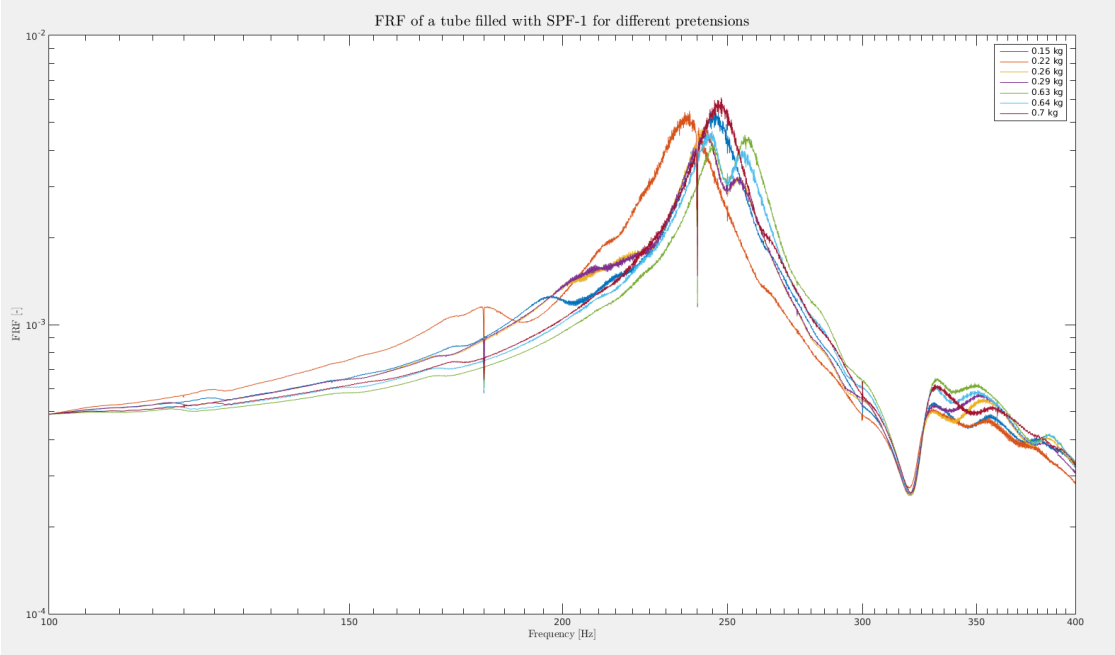

Figure 3.21. FRF of a tube filled with SPF-1 for different pretensions

Once again, the pretension has a non negligible impact of the main resonance frequency.

3.4 Comparison to the initial model

3.4.1 Single cell tube

Let's compare the results of a single cell tube filled with SPF-1 and the theoretical model.

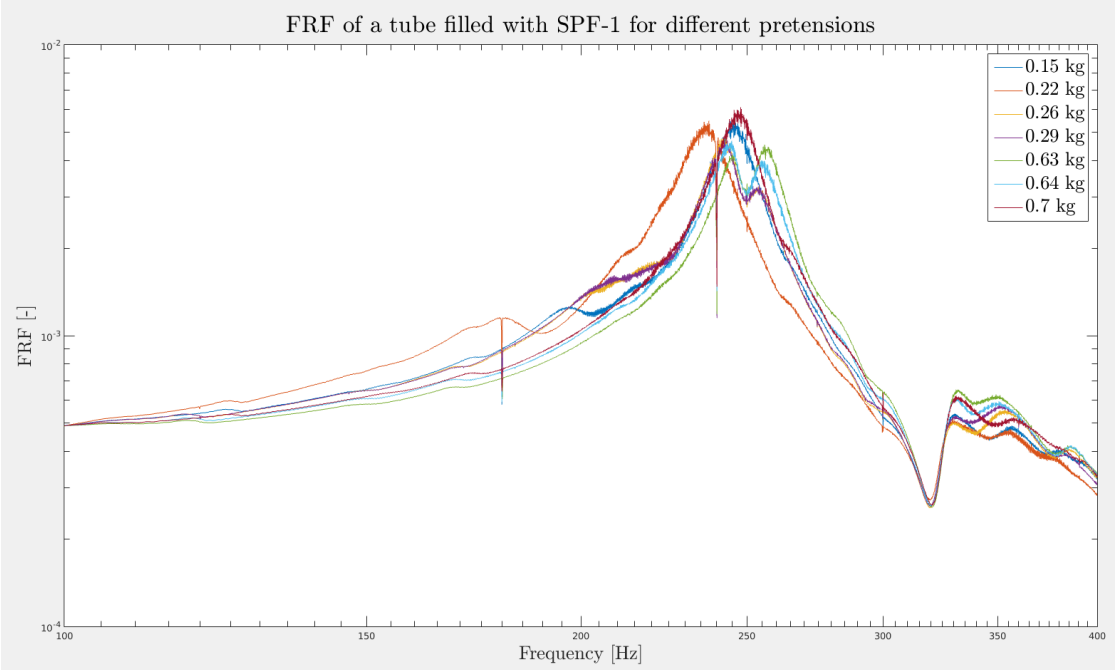

Figure 3.22. Comparison between single cell tube and model

For the right pre-tension, a good agreement between the output from the model and the experiment. The static stiffness was adjusted to match the one of the model. However,the resonance frequency is 20 Hz lower than what was found with the static stiffness measurements. This could be done to multiple factors:

1) The measurement of the static stiffness had a lower accuracy in the case of the tube filled with SPF-1 than in the case of a tube with air, given that the stiffness of a tube filled with liquid is increased by a lot. Therefore detected displacements was harder even with a 90 cm long tube.

2) The F^{2}MC tube is a non linear system. Therefore, it is hard to extrapolate the static results to the dynamic world. In particular, the when the tube is stretched the fibre angle angle is reduced as they align along the axis. When the tube is compressed, the fibre form an increased angle with the axis. The angle of the fibres not being constant changes the prediction of the resonance frequency.

3.4.2 Multi-cell tubes

Experiments were run for various different combinations of cells size and orifice size. A fair amount of runs were performed on three cell systems, given that it should have a fair amount of characteristic zeros and poles without taking too much time to make. However, the peaks and zeros that were expected never showed up.

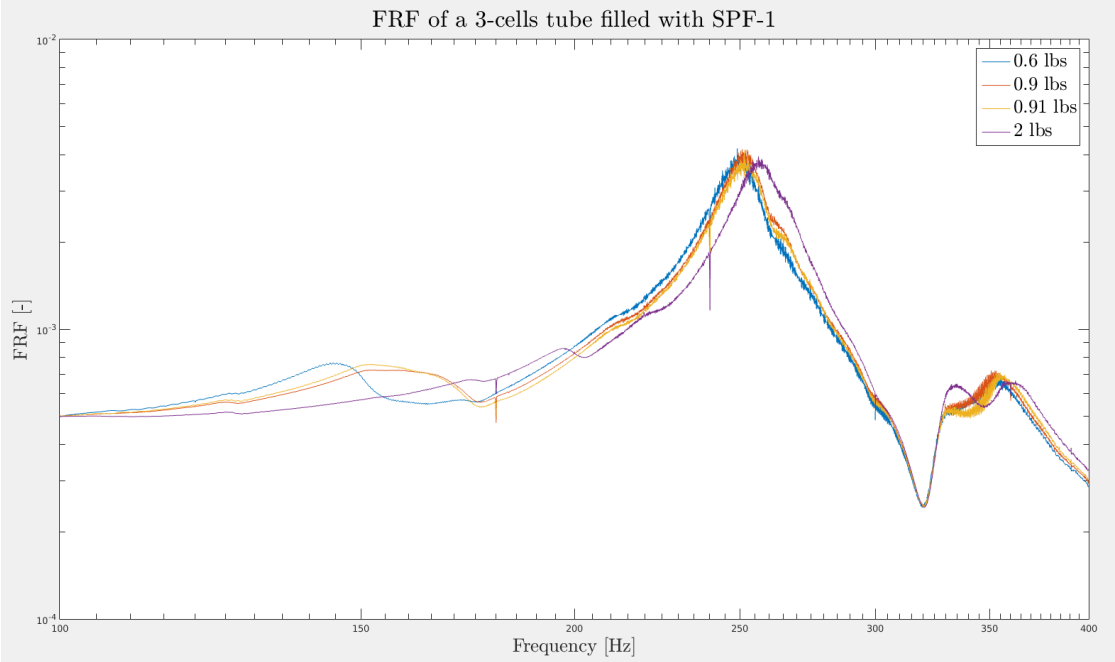

Figure 3.23. FRF of a three cells system for various pretensions

Now comparing to the single cell system and the theoretical response:

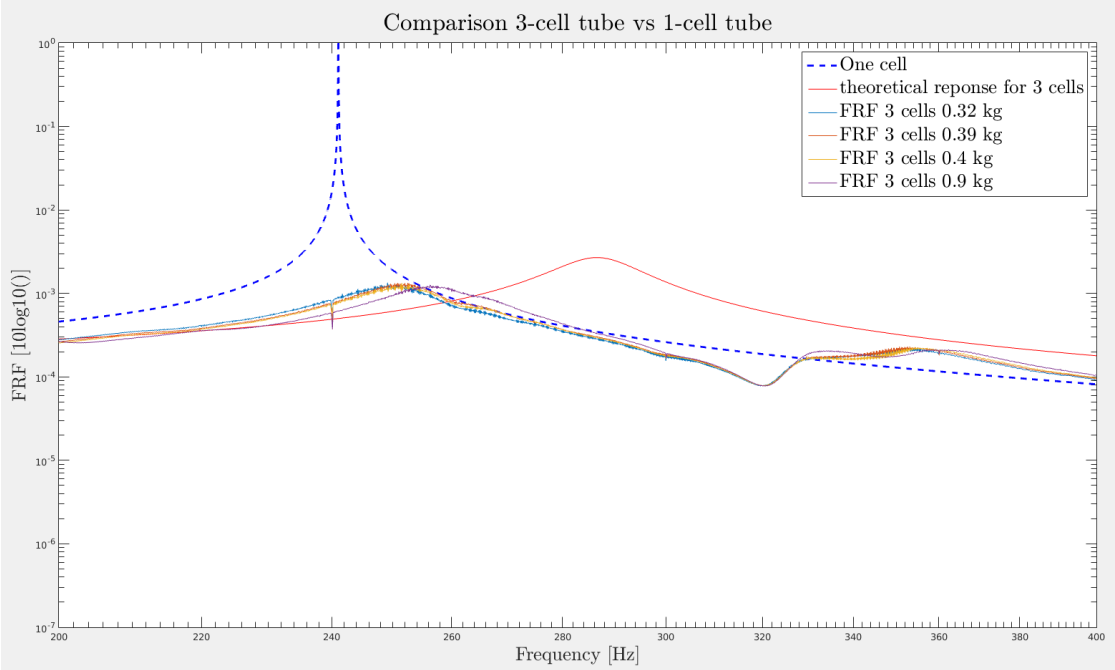

Figure 3.24. Comparison with theoretical response

The theory does not completely match the experimental results : more peaks should have been seen. In this case, the get a response which is close to the one found for a one tube system. A run up to 5000 Hz was then performed in order to check if some high frequency phenomenon would appear, but nothing showed up.

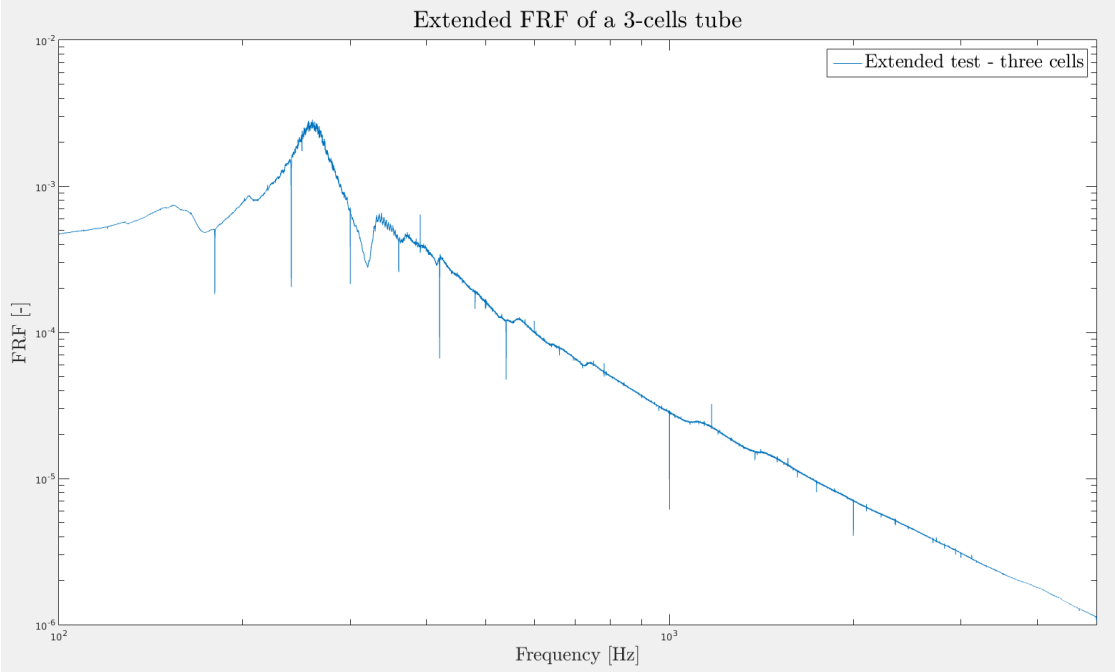

Figure 3.25. FRF of a three cells system for an extended frequency sweep

Discarding the 360 Hz zero which is due to the frame, there is no additional new peak. The vertical bars every 60 Hz are due to the electrical current. This experiment was repeated for a large number of cell properties and never yielded a different response.

3.4.3 Extended run of a 13 cells tube

Lastly, a 20 cm long 13 cells tubes with orifices that would reduce the inner diameter by 0.05" only. A high number of orifice was expensive to make and took multiple days to assemble without introducing any air bubble while filling the tube. Therefore, only one experiment with a really high number of cells was done. However, once again it did not yield the expected results. No additional peaks or valleys are seen on the FRF.

3.5 Impact of the resistance

Given that the experiment is run up to relatively high frequencies, the frequency correction previously used [5] might not be enough. Indeed, increasing slightly the resistance in the model dissipates completely any damping effect.

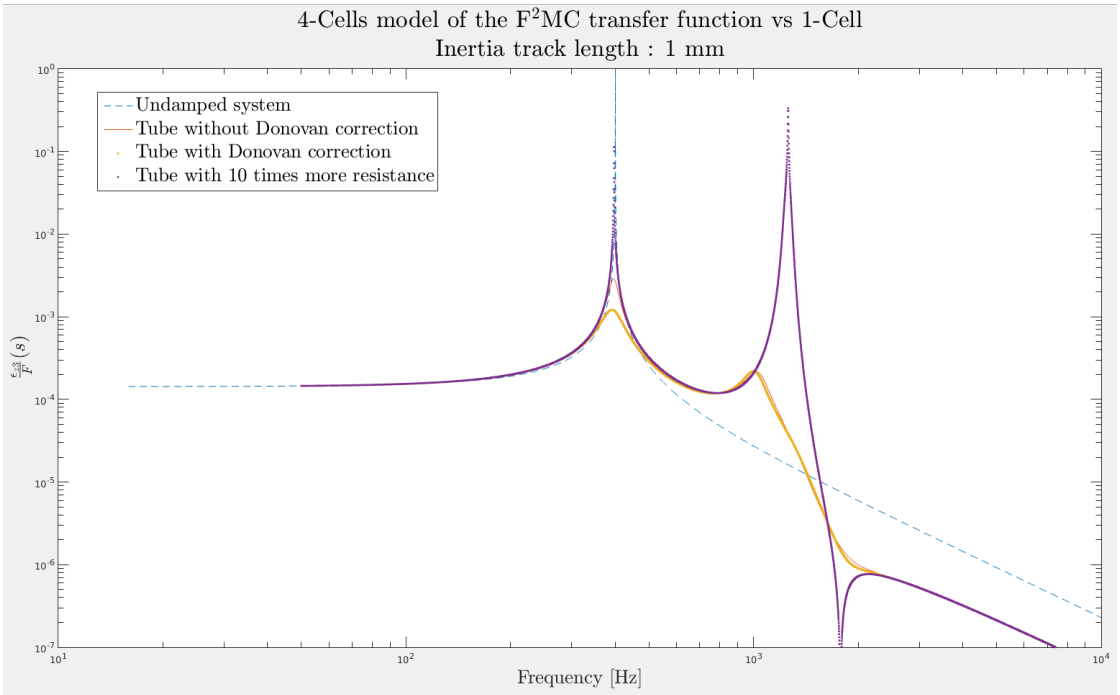

Figure 3.26. FRF of a thirteen cells system for an extended frequency sweep

Therefore the tube should exhibit multiple modes. But so far nothing as been found at higher frequencies.

Chapter 4
Conclusions and future work

4.1 Conclusions

In this research, the possibility of creating periodic F^{2}MC dampers that would target large portions of the frequency spectrum was investigated. First, the previous code used to modelize the frequency behaviour of a pack of F^{2}MC tubes was enhanced. Some physical parts of it were modified to take into account improved physical description of some phenomenons. Some other parts of the code were deeply redesigned to allow current computers to run it faster, in particular through the use of parallel computing. Consequently, it became possible to optimize the code and find patterns in how a slight change in the input can affect the output. Having this tool in hand, the concept of multi-cells F^{2}MC tube was investigated. Damping over a large area of the spectrum was expected. A lot of different tubes were made following a process that was constantly refined to provide the best sealing of the liquid. The porous nature of the walls at a thickness close to 200 μm was investigated and quantified. Measures were taken to ensure that this issue would be solved during the experimental runs. Then, a large number of different tubes undergoing longitudinal vibrations went under testing. However, despite all efforts and all the configurations that were tested, no concrete performance match with the model was found. Even if the single cell system performed as expected,

adding multiple cells did not change the frequency response by much. No more peaks of valleys were observed.

4.2 Future work

A few ways could be explored to improve the performances of the F^2MC tubes. The very first thing would be working with a different plastic. Polyurethane can apparently leak at low wall thickness and introduces a lot of leak issues. Even if its performances are supposed to be good, the plumbing issues are pretty frequents when dealing with F^2MC tubes and can be an important drawback. Likewise the tube diameter could be increased in order to deal more easily with the air bubbles. Some of them are in the order of 200-300 μm in diameter, making them really hard to extract due to the surface tension.

The fact that the experimental structure was horizontal was convenient to quickly run experiments but may make the reading of the results more complicated. Indeed, gravity is working against you, bending the tubes which do not have a high radial modulus. A vertical set-up would have gravity to work along the same axis as the shaker and could be managed more easily.

Another crucial issue was to be able to select the pretension to be applied to the system. The shaker was not always able to keep the pretension constant from one run to another, which meant constant low accuracy adjustments. A dedicated apparatus could be of some help in that regard, given how the performances vary with the pretension.

Lastly working with longer tubes could decrease the natural frequency due to a lower stiffness, maybe allowing us to work in better conditions.

Appendix A
Analytical solution for a dual-cell system

Here is the matrix to be solved to obtain the displacement in any point of the beam when two F^2MC tubes are embedded on it.

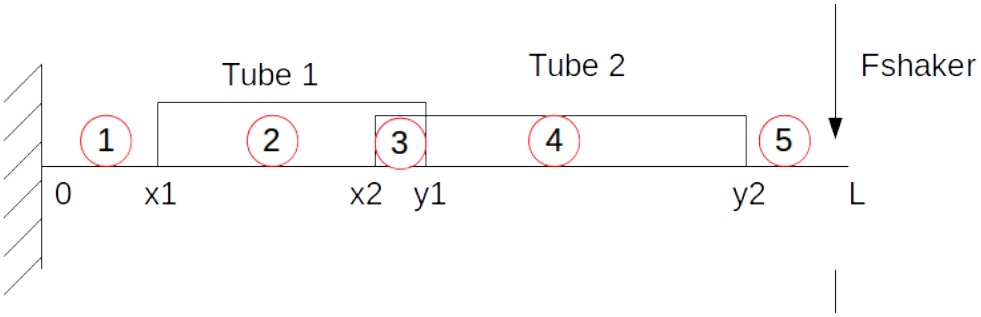

Figure A.1. Configuration of the tubes on the beam

Figure A.2. Matrix for 2 tubes

Appendix B
Analytical solution for a dual cell system

B.1 Remarks

Here is the analytical solution for a dual cell system. The solution was found by solving the system of linear equations with mupad. This result was then plugged into Matlab for further computations.

B.2 Transfer function of the system

Numerator:

$N(s) = I_w(\gamma S_q T_q \phi_2 - \gamma T_q^2 \phi_1 - \delta S_q^2 \phi_2 + \delta S_q T_q \phi_1)s^4 + ...$

$(2\gamma T_q \phi_1 - 2\gamma S_q \phi_2 - 2I_w T_q^2 \phi_1 + 2I_w S S_q^2 \phi_2 + 2I_w S_q T_q \phi_2 - 2I_w S S_q T_q \phi_1)s^2 + ...$

$4T_q \phi_1 - 4S_q \phi_2$

Denominator:

$D(s) = I_w(\gamma\delta' S_q T_q - \gamma\gamma' T_q^2 - \delta\delta' S_q^2 + \delta\gamma' S_q T_q)s^6 + ...$

$(2\gamma\gamma' T_q - \delta\gamma' S_q - \gamma\delta' S_q - I_w\gamma T_q^2 - I_w\gamma' T_q^2 + I_w\delta S_q T_q + I_w\delta' S_q T_q + I_w\delta S S_q^2 + I_w\delta' S S_q^2 - I_w\gamma S S_q T_q - I_w\gamma' S S_q T_q)s^4 + ...$

$(2\gamma T_q - 2\delta' S_q - \delta S_q + 2\gamma' T_q - I_w T_q^2 - I_w S^2 S_q^2 + \gamma S S_q - 2 I_w S S_q T_q) s^2 + ...$
$2T_q + 2SS_q$

As we can see, the size of the transfer function quickly increases to unmanageable sizes. There is a sort of pattern in the way it is built but the relationship between all the coefficient has not been found yet.

Appendix C
Leak measurement code

C.1 Arduino Code

Here is the Arduino code used to sample the sensors. The code was compiled using Arduino 1.0.6

```
#include <OneWire.h>
#include <DallasTemperature.h>
#include <dht.h>
#include <Wire.h> // Must include Wire library for I2C

//------------------------
// 1) Humidity sensor RHT03
//-------------------------
// Data wire for the RHT03 is connected to PIN 6
#define DHT22_PIN 6
#define DHT_LED 11
dht DHT;
```

```
//-----------------------------------
// 2) Temperature DS18B20
//-------------------------------------

// Data wire for the DS18B20 is connected to PIN 3
#define ONE_WIRE_DS18B20 3
#define T1_LED 8
#define T2_LED 9
#define T3_LED 10
#define TEMPRES 12 //precision of the measurements

// Setup a oneWire instance to communicate with any OneWire devices
// (not just Maxim/Dallas temperature ICs)
OneWire oneWire(ONE_WIRE_DS18B20);

// Pass our oneWire reference to Dallas Temperature.
DallasTemperature sensors(&oneWire);



byte DS18B20_ROM_1[8] = {0x28, 0x40, 0x2B, 0x31, 0x05, 0x00, 0x00, 0x11};
byte DS18B20_ROM_2[8] = {0x28, 0x38, 0x39, 0x31, 0x05, 0x00, 0x00, 0xD7};
byte DS18B20_ROM_3[8] = {0x28, 0x44, 0x7D, 0x30, 0x05, 0x00, 0x00, 0x4B};

int chk;

unsigned long int loopTime;

float humiTemp[2];
```

```
float temperature[3];



void setup(void)
{
  Serial.begin(115200);
  Serial.println("Starting up...");

  chk = DHT.read22(DHT22_PIN);

    switch (chk)
    {
      case DHTLIB_OK:
        Serial.println(F("RHT03 ok"));
        break;
      case DHTLIB_ERROR_CHECKSUM:
        Serial.println(F("RHT03 Checksum error"));
        break;
      case DHTLIB_ERROR_TIMEOUT:
        Serial.println(F("RHT03 Time out error"));
        break;
      default:
        Serial.println(F("RHT03 Unknown error"));
        break;
    }

   sensors.begin(); // Start up the library for the Temperature Sensors
   sensors.setWaitForConversion(0); // We'll not wait for conversion
```

```
   pinMode(DHT_LED, OUTPUT);
   pinMode(T1_LED, OUTPUT);
   pinMode(T2_LED, OUTPUT);
   pinMode(T3_LED, OUTPUT);

    Serial.println("Done!");
  }

  //Wire.begin(); //Join the bus as a master



void loop()
{
      loopTime = millis();
      sensors.requestTemperatures(); // Send the command to get temperatures -750
      temperature[0] = sensors.getTempC(DS18B20_ROM_1);
      temperature[1] = sensors.getTempC(DS18B20_ROM_2);
      temperature[2] = sensors.getTempC(DS18B20_ROM_3);

        chk = DHT.read22(DHT22_PIN);
        humiTemp[0] = DHT.humidity;
        humiTemp[1] = DHT.temperature;


      Serial.print(temperature[0]);Serial.print("\t");
      Serial.print(temperature[1]);Serial.print("\t");
      Serial.print(temperature[2]);Serial.print("\t");
```

```
      Serial.print(humiTemp[0]);Serial.print("\t");
      Serial.println(humiTemp[1]);
      blinkLed();

      delay(5000);
}



void blinkLed()
{
  for(int i=0; i<3; ++i)
  {
    if(temperature[i] > -5 && temperature[i] < 85)
    {
    digitalWrite(8+i, HIGH);
    }
    else
    {
      for (int j=0; j<20;++j)
      {
      digitalWrite(8+i, HIGH);
      delay(100);
      digitalWrite(8+i, LOW);
      delay(100);
      }
      break;
    }
  }
```

```
    if(humiTemp[0] > 0 && humiTemp[0] < 100 && humiTemp[1] > -5 && humiTemp[1] <
    {
      digitalWrite(11, HIGH);
    }
    else
    {
       for(int i = 0; i<3;++i)
      {
        digitalWrite(8+i, LOW);
      }
      for (int j=0; j<20;++j)
      {
       digitalWrite(11, HIGH);
      delay(100);
      digitalWrite(11, LOW);
      delay(100);
      }
    }

    delay(500);
  for(int i = 0; i<4;++i)
  {
    digitalWrite(8+i, LOW);
  }
    delay(500);
}
```

C.2 Raspberry Pi Code

Here is the Python code used to read the Arduino from the Raspberry Pi. The Raspberry Pi was running ArchLinux.

```
import serial
import os
import time

serialPortArduino = "/dev/ttyACM0"
serialPortArduinoSpeed = 115200
changeDirectory = "cd ~/masterThesis/"
forceCreateLogs = "touch sensors.data & > sensors.data"
pathDataFile = "sensors.data"
os.system(changeDirectory)
os.system(forceCreateLogs)

while True: # Check if Arduino if available
try:
arduino = serial.Serial(serialPortArduino, serialPortArduinoSpeed)
print("Communication with the Arduino established\n")
break
except serial.serialutil.SerialException as errorStreamOpen:
print("ERROR : ")
print(errorStreamOpen)
print("- Do you have enough priviledges? Auto retry in 1s\n")
time.sleep(1)
```

```
while True:
while arduino.inWaiting() != 0:
dataFile = open(pathDataFile, 'a')
bufferData = arduino.readline()
timestamp = time.clock()
if(timestamp>10):# Avoid the first sentences that are irelevant maths-wise
dataFile.write(str(timestamp))
dataFile.write("\t\t")
dataFile.write(bufferData)
print(bufferData)
dataFile.close()
```

Bibliography

[1] J. T. Szefi, *Helicopter gearbox isolation using periodically layered fluidic isolators*. Phd thesis, The Pennsylvania State University, University Park, August 2003.

[2] J. S. Pollard, "Helicopter gear noise and its transmission to the cabin," pp. 52/1–52/10, 1977.

[3] S. Y. B. C. W. K. Philen, M. and C. Rahn, "Variable stiffness adaptive structures utilizing hydraulically pressurized flexible matrix composites with valve control," in *Structural Dynamics and Materials Conference*, vol. 9, pp. 6387–6397, 2006.

[4] B. Zhu, *MODELING, DESIGN, AND EXPERIMENTAL TESTING OF INTEGRATED FLUIDIC FLEXIBLE MATRIX COMPOSITE STRUCTURES*. Phd thesis, The Pennsylvania State University, University Park, August 20014.

[5] T. B. S. M. Donovan FM, Jr., "One-dimensional computer analysis of oscillatory flow in rigid tubes," *Journal of Biomechanical Engineering*, vol. 113, no. 4, pp. 476–484, 1991.

[6] e. a. J. J. Coy, *IDENTIFICATION AND PROPOSED CONTROL OF HELICOPTER TRANSMISSION NOISE AT THE SOURCE*, pp. 1045–1065. Moffett Field, CA: NASA Ames Research Center, 1987.

[7] K. M. Rosen and H. K. Frint, "Advanced transmission component development," in *37th Annual Forum Proceedings - American Helicopter Society*, (New Orleans, LA), pp. 349–364, 1981.

[8] H. J. Marze and F. N. D'Ambra, "Helicopter internal noise treatment: Recent methodologies and practical application," in *Eleventh European Rotorcraft Forum*, (London, England), pp. 10.1–10.16, 1985.

[9] R. M. Hartman, *DYNAMICS APPROACH TO HELICOPTER TRANSMISSION NOISE REDUCTION AND IMPROVED RELIABILITY.* Zement-Kalk-Gips, 1973.

[10] L. S. Levin, "Reducing the cost impact of helicopter internal noise control," in *Proceedings of the 36th Annual Forum of the American Helicopter Society*, (Washington, DC), 1980.

[11] e. a. M. R. Jolly, "Adaptive control of helicopter cabin noise," in *Proceedings of the 1995 ASME International Mechanical Engineering Congress and Exposition*, (San Francisco, CA), pp. 837–842, November 1995.

[12] e. a. T. A. Millott, "Flight test of active gear-mesh noise control on the s-76 aircraft," in *Proceedings of the 1998 54th Annual Forum. Part 2*, (Washington, DC), pp. 241–249, May 1998.

[13] e. a. T. A. Millott, "Helicopter interior noise reduction by using active gearbox struts," in *12th AIAA/CEAS Aeroacoustics Conference*, (Cambridge, MA), pp. 2625–2634, May 2006.

[14] e. a. T. J. Sutton, "Active isolation of multiple structural waves on a helicopter gearbox support strut," *Journal of Sound and Vibration*, vol. 205, pp. 81–101, 1997.

[15] A. M. F. Zupan, M. and Fleck, "Actuator classification and selection âĂŤ the development of a database," *Advanced Engineering Materials*, vol. 4, no. 12, pp. 933–940, 2002.

[16] Z. B. B. C. E. Wimmer, B. M. and C. D. Rahn, "Actuation behavior of multilayer flexible matrix composite tubes with internal pressurization," in *Proc. SAMPE 2012 Conference and Exposition*, (Covina, CA), p. 15, 2012.

[17] P. M. B. C. W. K. Shan, Y. and C. Rahn, "Nonlinear-elastic finite axisymmetric deformation of flexible matrix composite membranes under internal pressure and axial force," *Composites Science and Technology*, vol. 66, no. 15, pp. 3053–3063, 2006.

[18] P. M. L. A. L. S. B. C. E. R. C. D. Shan, Y. and K. W. Wang, "Variable stiffness structures utilizing fluidic flexible matrix composites," *Journal of Intelligent Material Systems and Structures*, vol. 20, pp. 443–456, 2009.

[19] P. M. Zhang, Z. and W. Neu, "A biologically inspired artificial fish using flexible matrix composite actuators: analysis and experiment," *Smart Materials and Structures*, vol. 19, no. 9, p. 094017, 2010.

[20] R. C. Scarborough, L. and E. Smith, "Fluidic composite tunable vibration isolators," *ASME Journal of Vibration and Acoustics*, vol. 134, no. 3, p. 011010, 2012.

[21] B. J. Schwarz and M. H. Richardson, "Experimental modal analysis," *CSI Reliability Week*, vol. 36, no. 3, pp. 30–32, 1999.

[22] D. J. Ewins, "Modal testing: theory and practice," *Taunton: Research Studies Press*, vol. 36, no. 3, pp. 52–55, 1995.

[23] Z. F. Fu and J. He, "Modal analysis," *Butterworth-Heinemann*, 2001.

[24] S. Lekhnitskii, *Theory of elasticity of an anisotropic body.* San Francisco: Holden-Day Inc.

Vita

Bondoux Alexandre

Education

The Pennsylvania State University, University Park, PA (August 2015)
M.Sc. Aerospace Engineering
Ecole Centrale de Lyon, Ecully, France (August 2015)
M.Sc. General Engineering
Ecole Centrale de Lyon, Ecully, France (May 2012)
B.S. General Engineering